

Accuracy of the linear sampling method for inverse obstacle scattering: effect of geometrical and physical parameters

Nguyen Trung Thành* and Mourad Sini

Johann Radon Institute for Computational and Applied Mathematics (RICAM),
Austrian Academy of Sciences

Email addresses: trung-thanh.nguyen@oeaw.ac.at, mourad.sini@oeaw.ac.at

*Corresponding author.

April 14, 2010

Abstract

In this paper we investigate the effect of the geometry and the impedance of an obstacle as well as the anisotropy of the background medium on the accuracy of the linear sampling method for a two-dimensional acoustic inverse obstacle scattering problem with impedance boundary condition. The theoretical results show the dependence of the blowup rate of the limit (as the noise level tends to zero) of the so-called indicator function of the linear sampling method on these parameters. The analysis is done using asymptotic expansion of the solution to an interior problem. Concerning the *original* indicator function, we show that its blowup rate at a given internal point is of the same order as that of the limit if the noise level is small enough. Moreover, we also propose surface coating procedures for improving or destroying the accuracy in designing problems. Some numerical examples are given to illustrate the theoretical results.

Keywords: Linear sampling method, inverse obstacle scattering problem, impedance boundary condition, accuracy, asymptotic expansion, surface coating, numerics.

1 Introduction and motivation

We consider the scattering of time-harmonic acoustic waves by a two-dimensional bounded obstacle $D \in \mathbb{R}^2$ with smooth boundary (more precisely, ∂D is of class $C^{2,1}$ as required by theorem 3.2) when the scattered field u^s of an incident wave u^i can be represented by the following boundary value problem with impedance boundary condition [4]

$$\Delta u^s(x) + \kappa^2 u^s(x) = 0, \quad x \in \mathbb{R}^2 \setminus \bar{D}, \quad (1)$$

$$\left[\frac{\partial}{\partial \nu} + i\lambda(x) \right] [u^s(x) + u^i(x)] = 0, \quad x \in \partial D, \quad (2)$$

$$\lim_{r \rightarrow \infty} \sqrt{r} \left[\frac{\partial u^s(x)}{\partial r} - i\kappa u^s(x) \right] = 0, \quad r = |x|, \quad (3)$$

where κ is called the wave number, $\lambda(x)$ is referred to as the impedance of the boundary of the obstacle and ν is the outward unit normal vector of the boundary ∂D . In this system, equation (3) is called the Sommerfeld radiation condition, which guarantees the unique solvability of problem (1)–(2).

The asymptotic behavior of the scattered field u^s at infinity can be represented by

$$u^s(x) = \frac{e^{i\kappa r}}{\sqrt{r}} u^\infty(\hat{x}) + O(r^{-3/2}), \quad r \rightarrow \infty, \quad (4)$$

where $\hat{x} := x/r$ and u^∞ is an analytic function on the unit circle $\mathbb{S}^1 := \{x \in \mathbb{R}^2 : |x| = 1\}$ referred to as the *far field pattern* of the scattered field u^s . In the case of an incident plane wave, i.e., $u^i(x) = e^{i\kappa x \cdot d}$, with $d \in \mathbb{S}^1$ being the direction of propagation, we denote the far field pattern by $u^\infty(\hat{x}, d)$ to indicate its dependence on the incident direction d .

Problem (1)–(3), which is referred to as a forward scattering problem, is well-posed (see, e.g. [4]). In this paper, we consider the inverse problem of reconstructing the shape of the obstacle from the measured far field pattern $u^\infty(\hat{x}, d)$ for *all* incident directions $d \in \mathbb{S}^1$ and make use of the *linear sampling method* (LSM), which was introduced by Colton and Kirsch in 1996 [5], for solving it. Roughly speaking, in the LSM, an indicator function of one spatial variable is defined based on the solution of the so-called *far field equation*. The main idea of this method relies on the property that the indicator function is bounded in the interior of the obstacle D and explodes at the boundary of D as well as in the external region. For more details about this method, we refer the reader to [4, 9] and the references therein.

In our previous paper [15], we investigated the dependence of the accuracy of the LSM on the geometry of a sound-soft obstacle (with Dirichlet boundary condition). Both theoretical and numerical results showed that the blowup rate of the limit, as the noise level tends to zero, of the indicator function depends on the curvature of the obstacle boundary. This partly explained why obstacles with uniform curvatures can be detected with higher accuracy than obstacles with non-uniform curvatures. Similar results have also been obtained for the probe method [12, 13].

This work is an extension of our previous paper [15] to the case of impedance boundary condition with several additions. Firstly, we show that the blowup rate of the limit of the indicator function depends on not only the curvature but also the impedance of the obstacle boundary. To obtain this dependence, we also make use of the asymptotic expansions of the limit of the indicator function near the boundary in terms of the distance from a sampling point to the obstacle boundary as in [15]. Secondly, we investigate the blowup behavior of the original indicator function. Our analysis shows that for an arbitrary small positive value h , the blowup rate of the original indicator function at the points with distance to the boundary not less than h is of the same order as its limit when the noise level is less than a certain value δ^* , which depends on h (see theorem 3.7). This is an improved result compared to [15]. Thirdly, we study the effect of the anisotropy of the background medium on the accuracy of the LSM based on the results of the isotropic problem.

Both theoretical and numerical results show that, due to the effect of the geometry and the impedance, obstacles with uniform curvature and impedance can be reconstructed with high accuracy. In contrary, the reconstruction of obstacles with non-uniform curvature or oscillatory impedance is less accurate. The effect of the anisotropy of the background medium is even stronger since it also appears in the highest order singular term of the asymptotic expansion of the limit of the indicator function, which is not the case for the isotropic problem.

We note that, due to the limits of convergence results of the LSM for the general case [1], we confine our theoretical analysis to the case of purely imaginary impedance. However, our numerical tests show that the effect of the parameters is still clear even when the impedance is not purely imaginary.

Finally, given the dependence of (the limit of) the indicator function on the parameters, we propose surface coating procedures in order to enhance (or deteriorate) the uniformity of the blowup rate of (the limit of) the indicator function around the boundary. This makes the obstacle to be reconstructed more (or less) accurately in design problems. Our results suggest that in order to improve the accuracy, the impedance should be chosen so large that it dominates the effect of the curvature. To deteriorate the accuracy, we should choose a highly oscillatory impedance.

The rest of the paper is organized as follows. In section 2, we recall with some details the LSM and its convergence. The effect of the geometry and the impedance on the accuracy of the LSM is discussed in section 3 while in section 4 we analyze the effect of the anisotropy of the background medium. In section 5, we give some numerical tests to illustrate the theoretical results. In section 6, some conclusions are

drawn. The appendix provides the proof of the technical lemma 3.6.

2 The linear sampling method

Since in this paper we investigate the accuracy of the LSM for reconstructing the shape of the obstacle, let us recall its basis hereafter. For more details, we refer to [4] and the references therein.

Given the far field pattern $u^\infty(\hat{x}, d)$ of the scattered field of the forward problem (1)–(3) for incident plane waves $u^i(x) = e^{i\kappa x \cdot d}$, $d \in \mathbb{S}^1$, we define the so-called *far field operator* $F : L^2(\mathbb{S}^1) \rightarrow L^2(\mathbb{S}^1)$ corresponding to (1)–(3) as follows

$$(Fg)(\hat{x}) := \int_{\mathbb{S}^1} u^\infty(\hat{x}, d)g(d)ds(d) \text{ for } g \in L^2(\mathbb{S}^1), \hat{x} \in \mathbb{S}^1. \quad (5)$$

It has been proved that the far field operator F is linear, bounded, injective, compact and its range is dense in $L^2(\mathbb{S}^1)$ if κ^2 is not an eigenvalue of the corresponding interior problem (see, e.g. [4], chapter 4). Given the far field operator, the far field equation is defined by

$$(Fg_z)(\hat{x}) = \Phi^\infty(\hat{x}, z), \hat{x} \in \mathbb{S}^1, z \in \mathbb{R}^2, \quad (6)$$

where $\Phi^\infty(\hat{x}, z)$ is the far field pattern of the fundamental solution $\Phi(x, z)$ of the 2D Helmholtz equation given by

$$\Phi(x, z) = \frac{i}{4}H_0^{(1)}(\kappa|x - z|), \quad (7)$$

with $H_0^{(1)}$ being the Hankel function of the first kind of order zero. Using the asymptotic expansion of the Hankel function at infinity and (4), we obtain the explicit formula for the far field pattern of the fundamental solution

$$\Phi^\infty(\hat{x}, z) = \frac{e^{i\pi/4}}{\sqrt{8\pi\kappa}}e^{-i\kappa\hat{x}\cdot z}.$$

The following theorem is the fundamental result of the linear sampling method, see [4].

Theorem 2.1. *Let F be the far field operator defined by (5). Then we have*

1. *If $z \in D$, then for every $\epsilon > 0$, there exists a solution $g_z \in L^2(\mathbb{S}^1)$ of the inequality*

$$\|Fg_z - \Phi^\infty(\cdot, z)\|_{L^2(\mathbb{S}^1)} < \epsilon \quad (8)$$

such that $\lim_{z \rightarrow \partial D} \|g_z\|_{L^2(\mathbb{S}^1)} = +\infty$ and $\lim_{z \rightarrow \partial D} \|v_{g_z}\|_{H^1(D)} = +\infty$.

2. *If $z \notin D$, then for every $\delta > 0$ and $\epsilon > 0$, there exists a solution $g_z \in L^2(\mathbb{S}^1)$ of the inequality*

$$\|Fg_z - \Phi^\infty(\cdot, z)\|_{L^2(\mathbb{S}^1)} < \epsilon + \delta \quad (9)$$

such that $\lim_{\delta \rightarrow 0+} \|g_z\|_{L^2(\mathbb{S}^1)} = +\infty$ and $\lim_{\delta \rightarrow 0+} \|v_{g_z}\|_{H^1(D)} = +\infty$,

where v_{g_z} is the Herglotz wavefunction with density g_z defined by

$$v_{g_z}(x) = \int_{\mathbb{S}^1} e^{i\kappa x \cdot d} g_z(d) ds(d), \text{ for all } x \in \mathbb{R}^2. \quad (10)$$

In practice, the far field operator F cannot be given exactly since the measured far field pattern always contains noise. Therefore, F is replaced by F^δ with $\|F^\delta - F\| < \delta$, where δ is the noise level and $\|\cdot\|$ is the operator norm in $L^2(\mathbb{S}^1)$. Moreover, the two inequalities (8) and (9) are usually replaced by a regularized version of the far field equation. For example, using the Tikhonov regularization technique, we arrive at the following equation

$$[\alpha I + (F^\delta)^* F^\delta] g_{z,\alpha}^\delta = (F^\delta)^* \Phi^\infty(\cdot, z), \quad (11)$$

where I is the identity operator in $L^2(\mathbb{S}^1)$, $(F^\delta)^*$ is the adjoint operator of F^δ and $\alpha > 0$ is the regularization parameter. In this equation we write $g_{z,\alpha}^\delta$ to emphasize the dependence of the solution on the noise level and the regularization parameter. This equation is equivalent to the minimization problem [4]

$$g_{z,\alpha}^\delta = \operatorname{argmin}_{g \in L^2(\mathbb{S}^1)} \|F^\delta g - \Phi^\infty(\cdot, z)\|_{L^2(\mathbb{S}^1)}^2 + \alpha \|g\|_{L^2(\mathbb{S}^1)}^2. \quad (12)$$

Note that the regularization parameter α depends on δ and z and must be chosen in an appropriate way in order to guarantee the convergence of the solution of (12) to the solution of the far field equation (6). One of the optimal choices of this parameter is based on Morozov's discrepancy principle. That is, α is chosen by solving the implicit equation

$$\|F^\delta g_{z,\alpha}^\delta - \Phi^\infty(\cdot, z)\|_{L^2(\mathbb{S}^1)}^2 - \delta^2 \|g_{z,\alpha}^\delta\|_{L^2(\mathbb{S}^1)}^2 = 0. \quad (13)$$

Given the solution of the regularized far field equation, we can define an indicator function $I(z)$ with the expected property that its values in the interior and exterior of D are considerably different. For example, we can choose $I(z) := \|g_{z,\alpha}^\delta\|_{L^2(\mathbb{S}^1)}$ or $I(z) := \|g_{z,\alpha}^\delta\|_{L^2(\mathbb{S}^1)}^{-1}$.

Based on Theorem 2.1 and the above analysis, the common implementation of the linear sampling algorithm with Tikhonov regularization can be briefly described as follows

1. Choose a set of sampling points in a region covering the expected obstacle.
2. For each sampling point z , find a regularization parameter α and an approximate solution of the regularized far field equation (11) such that (13) is satisfied.
3. Calculate the indicator function $I(z)$.
4. Use some cut-off value C to determine an approximation D_a of D by asserting that $z \in D_a$ iff $I(z) < C$ (or $I(z) > C$, depending the behavior of the chosen indicator function).

Note that apart from the cut-off procedure for choosing the approximation of the shape, there are also other post-processing methods available in the literature, see e.g. [3].

2.1 Convergence of the LSM

It is clear that the solution of the regularized far field equation (11) is finite in the whole space. To use this solution to reconstruct the obstacle, we show that it converges (as the noise level δ and the regularization parameter α tend to zero) to a function that is moderate inside the obstacle and blows up at the boundary as well as in the exterior region.

In the next section, we will investigate the roles of geometrical properties as well as the surface impedance $\lambda(x)$ of the obstacle on the blowup rate of the indicator function. For this purpose, we not only use the far field pattern of the fundamental solution (*monopole*) but also its first derivatives (*dipoles*) and second derivatives (*tripoles*) as the right hand side of the regularized far field equation (12). Therefore in this section, we consider the solution to the following general regularized far field equation

$$(\alpha I + (F^\delta)^* F^\delta) g_{z,\alpha}^\delta = (F^\delta)^* \psi^\infty(\cdot, z), \quad (14)$$

where $\psi^\infty(\cdot, z)$ is the far field pattern of the function $\psi(x, z)$ which is one of the following cases

$$\begin{aligned} 1) \text{ (monopole)} \quad & \psi(x, z) = \Phi(x, z) \\ 2) \text{ (dipoles)} \quad & \psi(x, z) = \frac{\partial \Phi(x, z)}{\partial z_j}, j \in \{1, 2\} \\ 3.1) \text{ (tripoles)} \quad & \psi(x, z) = \frac{\partial^2 \Phi(x, z)}{\partial z_1^2}, \quad 3.2) \quad \psi(x, z) = \frac{\partial^2 \Phi(x, z)}{\partial z_1 \partial z_2}. \end{aligned} \tag{15}$$

To prove the convergence of the LSM, let us define two more operators. Firstly, we consider the general forward scattering problem

$$\begin{cases} \Delta u(x) + \kappa^2 u(x) = 0, & x \in \mathbb{R}^2 \setminus \bar{D}, \\ \left[\frac{\partial}{\partial \nu} + i\lambda(x) \right] u(x) = f(x), & x \in \partial D, \\ \lim_{r \rightarrow \infty} \sqrt{r} \left(\frac{\partial u(x)}{\partial r} - i\kappa u \right) = 0, & r = |x|, \end{cases} \tag{16}$$

and denote by B the linear operator maps the boundary data $f \in H^{-1/2}(\partial D)$ onto the far field pattern u^∞ of (16). We also define the operator $H : L^2(\mathbb{S}^1) \rightarrow H^{-1/2}(\partial D)$ by

$$Hg = \frac{\partial v_g}{\partial \nu} |_{\partial D} + i\lambda(\cdot)v_g |_{\partial D}.$$

Then we have the factorization of the far field operator [4]

$$F = -B \cdot H. \tag{17}$$

The convergence of the LSM was addressed in [1, 2, 8] for the case of Dirichlet boundary condition and Tikhonov regularization method. In [1, 2], the authors used the well-justified factorization method (see [9]) to prove the convergence of the Herglotz wavefunction $v_{g_{z,\alpha}^\delta}$, with the solution to the regularized equation (11) being its density, to $-\Phi(\cdot, z)$ in $H^{1/2}(\partial D)$ as the noise level δ tends to zero for $z \in D$ if the regularization parameter is chosen such that $\alpha \rightarrow 0$ and $\delta/\alpha^{3/2} \rightarrow 0$ as δ tends to zero. This implies that the Herglotz wavefunction explodes near ∂D . For $z \notin D$, the authors also showed that $|v_{g_{z,\alpha}^\delta}(z)|$ (i.e., in the absence of noise) tends to infinity (see also [9]). The authors also noted that the convergence is true when the far field operator F is normal. As pointed out in [9], for the case of impedance boundary condition, *the far field operator F is normal only if the surface impedance $\lambda(x)$ is purely imaginary*. In this case, using the same arguments as in theorem 4.1 of [1] and theorem 3.1 of [2], we can justify the following result.

Theorem 2.2. *Assume that the surface impedance $\lambda(x)$, $x \in \partial D$, is purely imaginary. Consider an arbitrary but fixed sampling point $z \in D$ and let $v_{g_{z,\alpha}^\delta}(x)$, $x \in \mathbb{R}^2$, be the Herglotz wavefunction with density $g_{z,\alpha}^\delta$ being the solution to the regularized far field equation (14). Moreover, the regularization parameter is chosen so that both α and $\delta/\alpha^{3/2}$ tend to zero as $\delta \rightarrow 0$. Then we have*

$$Hg_{z,\alpha}^\delta \longrightarrow - \left(\frac{\partial \psi(\cdot, z)}{\partial \nu} |_{\partial D} + i\lambda(\cdot)\psi(\cdot, z) |_{\partial D} \right) \tag{18}$$

in the space $H^{-1/2}(\partial D)$. Here ψ is one of the functions defined in (15).

Remark 2.1. Although the convergence of the LSM when the impedance is not purely imaginary has not been proved, our numerical tests show that the effect of the geometry and impedance on the accuracy of the LSM can still be seen in this case.

2.2 Accuracy issue of the LSM

In numerical implementations, the cut-off constant C is usually fixed for all sampling points. However, the blowup rate of the indicator function $I(z)$ may depend on physical and geometrical properties of the boundary of the obstacle. Hence, the accuracy of the reconstruction may depend on the properties of the boundary ∂D . In our previous paper [15], we showed that the accuracy of the LSM depends on the curvature of the boundary of the obstacle in case of a sound-soft acoustic obstacle. In this paper, we show that the accuracy of the LSM depends on not only the geometrical but also the physical properties of the obstacle. Moreover, we will show that it also depends on the anisotropy of the background medium.

3 Effect of the geometry and the impedance on the accuracy

In this section, we analyze the roles of the geometry and impedance of the obstacle boundary on the accuracy of the LSM. We first show in subsection 3.1 that the blowup rate of the limit of the indicator function depends on the curvature as well as the surface impedance of the obstacle boundary. Then in subsection 3.2, we give some analysis on the blowup rate of the original indicator function itself. This helps understanding the roles of these factors in the accuracy of the LSM. Given the dependence of (the limit of) the indicator function on the geometry and the impedance, we propose coating methods to either enhance or destroy the accuracy. The analysis given in this section is based on asymptotic expansions of the solution to an interior problem.

We note that, since v_g satisfies the Helmholtz equation in the whole space for any density $g \in L_2(\mathbb{S}^1)$, the following result is a straightforward consequence of Theorem 2.2.

Lemma 3.1. *Under the assumptions of Theorem 2.2, the following convergence holds true for the Herglotz wavefunction $v_{g_{z,\alpha}^\delta}$*

$$\lim_{\delta \rightarrow 0} |v_{g_{z,\alpha}^\delta}(z) - \varphi(z, z)| = 0, \quad z \in D, \quad (19)$$

where $\varphi(x, z)$ is the solution of the interior boundary value problem

$$\begin{cases} \Delta \varphi(x, z) + \kappa^2 \varphi(x, z) = 0, & x \in D, \\ \frac{\partial \varphi(x, z)}{\partial \nu} + i\lambda(x)\varphi(x, z) = - \left[\frac{\partial \psi(x, z)}{\partial \nu} + i\lambda(x)\psi(x, z) \right], & x \in \partial D. \end{cases} \quad (20)$$

3.1 Asymptotic expansion of $\varphi(z, z)$

To understand the dependence of the Herglotz wavefunction $v_{g_{z,\alpha}^\delta}$ on the geometry and the impedance, we investigate the asymptotic behavior of $\varphi(z, z)$ as $z \in D$ tends to an arbitrary but fixed point $a \in \partial D$. For this, we need to assume that $\partial D \in C^{2,1}$, i.e., there exists a rigid coordinate transformation under which $a = 0$ and there exists a positive value r such that $\bar{D} \cap B(0, r) = \{\bar{x} \in \mathbb{R}^2 : \bar{x}_2 > f_a(\bar{x}_1)\}$, where \bar{D} is the considered domain in the new coordinate system and the function $f_a \in C^{2,1}[-r, r]$ satisfies $f_a(0) = 0$, $f'_a(0) = 0$. The main result of this section is the following theorem.

Theorem 3.2. *Suppose that the boundary of the obstacle D is of class $C^{2,1}$. Let a be an arbitrary point on ∂D with out-ward unit normal vector $\nu(a)$. We denote by $C(a, \theta)$ the cone with vertex a , axis $-\nu(a)$ and an arbitrary but fixed angle $\theta \in [0, \frac{\pi}{2})$. Then, the solution $\varphi(x, z)$ of the interior problem (20), with $\psi(x, z)$ given by (15), has the following asymptotic expansion as $z \in D \cap C(a, \theta)$ tends to a :*

1) For $\psi = \Phi(x, z)$:

$$\varphi(z, z) = -\frac{1}{2\pi} \ln |(z - a) \cdot \nu(a)| + O(1). \quad (21)$$

2) For $\psi = \frac{\partial}{\partial z_j} \Phi(x, z)$, $j \in \{1, 2\}$:

$$\varphi(z, z) = \frac{\nu_j(a)}{4\pi|(z-a) \cdot \nu(a)|} + O(1). \quad (22)$$

3.1) For $\psi = \frac{\partial^2}{\partial z_1^2} \Phi(x, z)$:

$$\begin{aligned} \varphi(z, z) = & -\frac{\nu_2^2(a) - \nu_1^2(a)}{8\pi|(z-a) \cdot \nu(a)|^2} + \frac{[\nu_2^2(a) - \nu_1^2(a)][8i\lambda(a) + f_a''(0)]}{16\pi|(z-a) \cdot \nu(a)|} \\ & - \frac{\nu_1(a)\nu_2(a)f_a''(0)}{4\pi|(z-a) \cdot \nu(a)|} \tan \theta_{za} + O((\ln |(z-a) \cdot \nu(a)|)^2). \end{aligned} \quad (23)$$

3.2) For $\psi = \frac{\partial^2}{\partial z_1 \partial z_2} \Phi(x, z)$:

$$\begin{aligned} \varphi(z, z) = & \frac{\nu_1(a)\nu_2(a)}{4\pi|(z-a) \cdot \nu(a)|^2} - \frac{\nu_1(a)\nu_2(a)[8i\lambda(a) + f_a''(0)]}{8\pi|(z-a) \cdot \nu(a)|} \\ & - \frac{(\nu_2^2(a) - \nu_1^2(a))f_a''(0)}{8\pi|(z-a) \cdot \nu(a)|} \tan \theta_{za} + O((\ln |(z-a) \cdot \nu(a)|)^2). \end{aligned} \quad (24)$$

Here θ_{za} is the angle between the vector $z-a$ and $\nu(a)$ which is defined to be positive if the rotation from $z-a$ to $\nu(a)$ is clockwise and negative if the rotation is anticlockwise.

Remark 3.1. Similar to the case of Dirichlet boundary condition presented in [15], we also see that in the case of tripoles (23) and (24), the curvature of the boundary ∂D (represented by $f_a''(0)$) is involved in the first order singularity of $\varphi(z, z)$. Moreover, the impedance plays a similar role as the curvature. If we consider the combined function

$$\varphi(z, z) = [\varphi_{3,1}^2(z, z) + \varphi_{3,2}^2(z, z)]^{1/2},$$

where $\varphi_{3,1}^2(z, z)$ and $\varphi_{3,2}^2(z, z)$ are given by (23) and (24), respectively, and approach a in the normal direction, i.e., $z = a - h\nu(a)$, $h > 0$, then it follows from (23) and (24) that

$$\varphi(z, z) = \left[\frac{1}{64\pi^2 h^4} - \frac{8i\lambda(a) + f_a''(0)}{64\pi^2 h^3} + O\left(\frac{1}{h^2}\right) \right]^{1/2}, \text{ for } h \rightarrow 0. \quad (25)$$

This equation shows that if the curvature and the impedance are uniform or they cancel each other in the highest singular term containing them, the level curves of $\varphi(z, z)$ should provide similar shapes as ∂D (up to the effect of the lower order terms) when they are "close enough" to the boundary. On the contrary, if the curvature (or the impedance) is non-uniform (oscillatory), the blowup rate may be non-uniform around the obstacle boundary. This analysis not only helps partly explain the roles of the curvature and the impedance of the obstacle boundary on the accuracy of the linear sampling method but also helps us in choosing a *coating procedure* in design problems in such a way that the obstacle can be more or less accurately reconstructed.

For the role of the curvature (similar for the impedance) in the cases of the monopole and dipoles, see Remark 3.3 in [15].

Proof of Theorem 3.2. We divide the proof of the theorem into 4 steps as follows.

Step 1: Since we only analyze the value $\varphi(z, z)$ for z near $a \in \partial D$, we first approximate, for the simplicity of the analysis, the impedance $\lambda(x)$ in (20) by its value $\lambda(a)$ at $x = a$, i.e., we compare $\varphi(x, z)$ with the solution $\varphi_a(x, z)$ of the following problem

$$\begin{cases} \Delta \varphi_a(x, z) + \kappa^2 \varphi_a(x, z) = 0, & x \in D, \\ \left[\frac{\partial}{\partial \nu} + i\lambda(a) \right] \varphi_a(x, z) = - \left[\frac{\partial}{\partial \nu} + i\lambda(a) \right] \psi(x, z), & x \in \partial D. \end{cases} \quad (26)$$

Step 2: Next, we note that the singularity of the fundamental solution of the Helmholtz equation in (26) is of the same order as that of the Laplace equation. Hence, to make the analysis easier, we replace the former by the latter. That is, we compare $\varphi_a(x, z)$ with the solution $\varphi_{a,\Gamma}(x, z)$ of the following problem

$$\begin{cases} \Delta\varphi_{a,\Gamma}(x, z) + \kappa^2\varphi_{a,\Gamma}(x, z) = 0, & x \in D, \\ \left[\frac{\partial}{\partial\nu} + i\lambda(a)\right]\varphi_{a,\Gamma}(x, z) = -\left[\frac{\partial}{\partial\nu} + i\lambda(a)\right]\Gamma(x, z), & x \in \partial D, \end{cases} \quad (27)$$

where $\Gamma(x, z)$ is the fundamental solution of the Laplace equation or its derivatives. From (15), we have the following cases

$$\begin{aligned} 1) \text{ (monopole)} \quad & \Gamma(x, z) = \frac{1}{2\pi} \ln \frac{1}{|x-z|} =: \Gamma_0(x, z) \\ 2) \text{ (dipoles)} \quad & \Gamma(x, z) = \frac{\partial\Gamma_0(x, z)}{\partial z_j}, j \in \{1, 2\} \\ 3.1) \text{ (tripoles)} \quad & \Gamma(x, z) = \frac{\partial^2\Gamma_0(x, z)}{\partial z_1^2}, \quad 3.2) \quad \Gamma(x, z) = \frac{\partial^2\Gamma_0(x, z)}{\partial z_1\partial z_2}. \end{aligned} \quad (28)$$

Step 3: Compare $\varphi_{a,\Gamma}(x, z)$ with the solution $\varphi_{a,\Gamma}^0(x, z)$ of the following problem for the Laplace equation

$$\begin{cases} \Delta\varphi_{a,\Gamma}^0(x, z) = 0, & x \in D, \\ \left[\frac{\partial}{\partial\nu} + i\lambda(a)\right]\varphi_{a,\Gamma}^0(x, z) = -\left[\frac{\partial}{\partial\nu} + i\lambda(a)\right]\Gamma(x, z), & x \in \partial D. \end{cases} \quad (29)$$

The results of these three steps are summarized in the following lemma. For its proof, see Lemmas 3.5 and 3.6 of [14].

Lemma 3.3. *For $z \in D \cap C(a, \theta)$ closed enough to a , we have the following approximation for the monopole and the dipoles*

$$|\varphi(z, z) - \varphi_{a,\Gamma}^0(z, z)| = O(1), \quad (30)$$

and for the tripoles, we have

$$|\varphi(z, z) - \varphi_{a,\Gamma}^0(z, z)| = O(\ln(|z-a|)^2). \quad (31)$$

Step 4: Finally, we investigate the asymptotic expansion of $\varphi_{a,\Gamma}^0(z, z)$ as z tends to the point $a \in \partial D$. For this purpose, we consider the coordinate transformation $\bar{x} = R(x-a)$, where R is the rotation matrix defined by

$$R = \begin{pmatrix} -\nu_2(a) & \nu_1(a) \\ -\nu_1(a) & -\nu_2(a) \end{pmatrix}$$

where $\nu(a) = (\nu_1(a), \nu_2(a))^T$ is the out-ward unit normal vector of ∂D at the point a . Under this coordinate transformation, the point a becomes the origin and its normal vector $\nu(a)$ becomes $(0, -1)^T$ in the \bar{x} -coordinate system, i.e., $R\nu(a) = (0, -1)^T$ (see Figure 1(a)). We denote by \bar{D} the obstacle in the new coordinate system. We also denote by $\bar{\varphi}(\bar{x}, \bar{z}) = \varphi_{a,\Gamma}^0(x, z)$ and $\bar{\Gamma}(\bar{x}, \bar{z}) = \Gamma(x, z)$. In the \bar{x} -coordinate system, the function $\bar{\varphi}$ satisfies the system

$$\begin{cases} \Delta\bar{\varphi}(\bar{x}, \bar{z}) = 0, & \bar{x} \in \bar{D}, \\ \left[\frac{\partial}{\partial\nu(\bar{x})} + i\lambda(a)\right]\bar{\varphi}(\bar{x}, \bar{z}) = -\left[\frac{\partial}{\partial\nu(\bar{x})} + i\lambda(a)\right]\bar{\Gamma}(\bar{x}, \bar{z}), & \bar{x} \in \partial\bar{D}. \end{cases} \quad (32)$$

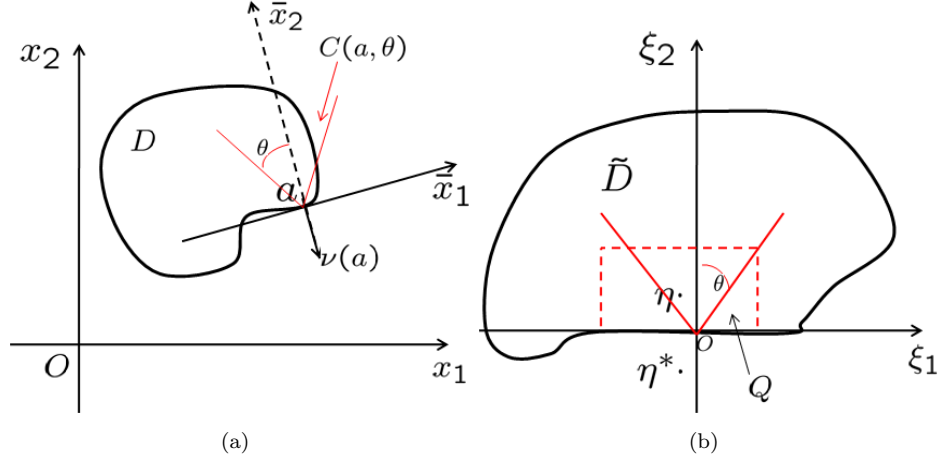


Figure 1: Coordinate transformations: (a) from x to \bar{x} ; (b) in ξ -coordinate system.

It follows from (28) that $\bar{\Gamma}(\bar{x}, \bar{z})$ is one of the following cases

$$\begin{aligned}
 1) \text{ (monopole)} \quad & \bar{\Gamma}(\bar{x}, \bar{z}) = \Gamma_0(x, z) = \frac{1}{2\pi} \ln \frac{1}{|x - z|} = \frac{1}{2\pi} \ln \frac{1}{|\bar{x} - \bar{z}|} \\
 2) \text{ (dipoles)} \quad & \bar{\Gamma}(\bar{x}, \bar{z}) = \frac{\partial \Gamma_0(x, z)}{\partial z_j} = (R_j^c)^T \nabla_{\bar{z}} \Gamma_0(\bar{x}, \bar{z}), j \in \{1, 2\} \\
 3.1) \text{ (tripoles)} \quad & \bar{\Gamma}(\bar{x}, \bar{z}) = \frac{\partial^2 \Gamma_0(x, z)}{\partial z_1^2} = [\nu_2^2(a) - \nu_1^2(a)] \frac{\partial^2 \Gamma_0(\bar{x}, \bar{z})}{\partial \bar{z}_1^2} + 2\nu_1(a)\nu_2(a) \frac{\partial^2 \Gamma_0(\bar{x}, \bar{z})}{\partial \bar{z}_1 \partial \bar{z}_2} \\
 3.2) \quad & \bar{\Gamma}(\bar{x}, \bar{z}) = \frac{\partial^2 \Gamma_0(x, z)}{\partial z_1 \partial z_2} = -2\nu_1(a)\nu_2(a) \frac{\partial^2 \Gamma_0(\bar{x}, \bar{z})}{\partial \bar{z}_1^2} + [\nu_2^2(a) - \nu_1^2(a)] \frac{\partial^2 \Gamma_0(\bar{x}, \bar{z})}{\partial \bar{z}_1 \partial \bar{z}_2}.
 \end{aligned} \tag{33}$$

Here $(R_j^c)^T$ is the transpose of the j th-column of the rotation matrix R . We note that for the cases 2, 3.1, 3.2, we only have to derive the asymptotic expansion of $\bar{\varphi}$ when $\bar{\Gamma}$ is given by

$$\begin{aligned}
 2) \quad & \bar{\Gamma}(\bar{x}, \bar{z}) = \frac{\partial \Gamma_0(\bar{x}, \bar{z})}{\partial \bar{z}_j}, j \in \{1, 2\} \\
 3.1) \quad & \bar{\Gamma}(\bar{x}, \bar{z}) = \frac{\partial^2 \Gamma_0(\bar{x}, \bar{z})}{\partial \bar{z}_1^2}, \quad 3.2) \quad \bar{\Gamma}(\bar{x}, \bar{z}) = \frac{\partial^2 \Gamma_0(\bar{x}, \bar{z})}{\partial \bar{z}_1 \partial \bar{z}_2}
 \end{aligned}$$

and then use the superposition of the solutions of (32) and the equalities (33) to arrive at the equations (22)–(24).

For studying the asymptotic expansion of $\bar{\varphi}(\bar{z}, \bar{z})$, we first extend f_a to the whole \bar{x}_1 -axis with constant values far from the origin. For the sake of simplicity, we still denote this extended function by f_a . Let us consider the coordinate transformation $\xi = \Theta(\bar{x})$ defined by

$$\begin{cases} \xi_1 = \bar{x}_1, \\ \xi_2 = \bar{x}_2 - f_a(\bar{x}_1). \end{cases} \tag{34}$$

Under this transformation, the domain \bar{D} is transformed into the domain \tilde{D} as shown in Figure 1(b) with a part of its boundary near the origin lies on the ξ_1 -axis. We denote by $\tilde{\varphi}(\xi, \eta) = \bar{\varphi}(\bar{x}, \bar{z})$, with $\xi = \Theta(\bar{x})$ and $\eta = \Theta(\bar{z})$. We have

$$\frac{\partial \bar{\varphi}(\bar{x}, \bar{z})}{\partial \nu(\bar{x})} = J^T \nabla_{\xi} \tilde{\varphi}(\xi, \eta) \cdot \frac{J^T \nu(\xi)}{|J^T \nu(\xi)|} = M \nabla_{\xi} \tilde{\varphi}(\xi, \eta) \cdot \nu(\xi) \frac{1}{|J^T \nu(\xi)|},$$

where J is the Jacobian of the coordinate transformation, i.e.

$$J = \begin{pmatrix} \frac{\partial \xi_1}{\partial \bar{x}_1} & \frac{\partial \xi_1}{\partial \bar{x}_2} \\ \frac{\partial \xi_2}{\partial \bar{x}_1} & \frac{\partial \xi_2}{\partial \bar{x}_2} \end{pmatrix} = \begin{pmatrix} 1 & 0 \\ -f'_a(\xi_1) & 1 \end{pmatrix} \quad (35)$$

and $M = JJ^T$. It follows from (35) that

$$M = \begin{pmatrix} 1 & -f'_a(\xi_1) \\ -f'_a(\xi_1) & 1 + (f'_a(\xi_1))^2 \end{pmatrix}. \quad (36)$$

Therefore, the function $\tilde{\varphi}(\xi, \eta)$ satisfies the following problem in the ξ -coordinate system

$$\begin{cases} \nabla \cdot [M \nabla \tilde{\varphi}(\xi, \eta)] = 0, & \xi \in \tilde{D}, \\ M \nabla_{\xi} \tilde{\varphi}(\xi, \eta) \cdot \nu(\xi) + i\lambda(a) |J^T \nu(\xi)| \tilde{\varphi}(\xi, \eta) \\ = - [\nabla_{\bar{x}} \bar{\Gamma}(\Theta^{-1}(\xi), \Theta^{-1}(\eta)) \cdot J^T \nu(\xi) + i\lambda(a) |J^T \nu(\xi)| \bar{\Gamma}(\Theta^{-1}(\xi), \Theta^{-1}(\eta))], & \xi \in \partial \tilde{D}. \end{cases} \quad (37)$$

It is clear from (36) that M is positive definite, hence (37) is well-defined. To study the asymptotic behavior of $\tilde{\varphi}(\xi, \eta)$, we compare it with the solution $\omega^+(\xi, \eta)$ of the following boundary value problem in the upper half space

$$\begin{cases} \Delta \omega^+(\xi, \eta) = 0, & \xi \in \mathbb{R}_+^2, \\ \left[\frac{\partial}{\partial \nu} + i\lambda(a) \right] \omega^+(\xi, \eta) = - \left[\frac{\partial}{\partial \nu} + i\lambda(a) \right] \bar{\Gamma}(\xi, \eta), & \xi \in \partial \mathbb{R}_+^2. \end{cases} \quad (38)$$

The asymptotic behavior of the function $\omega^+(\xi, \eta)$ is given in the following lemma. For its proof, see [14].

Lemma 3.4. *For the solution of (38) we have the following asymptotic expansions as $\eta \rightarrow 0$*

- 1) If $\bar{\Gamma}(\bar{x}, \bar{z}) = \Gamma_0(\bar{x}, \bar{z})$, then $\omega^+(\eta, \eta) = \frac{1}{2\pi} \ln \eta_2 + O(1)$.
- 2.1) If $\bar{\Gamma}(\bar{x}, \bar{z}) = \frac{\partial \Gamma_0(\bar{x}, \bar{z})}{\partial \bar{z}_1}$, then $\omega^+(\eta, \eta) = O(1)$.
- 2.2) If $\bar{\Gamma}(\bar{x}, \bar{z}) = \frac{\partial \Gamma_0(\bar{x}, \bar{z})}{\partial \bar{z}_2}$, then $\omega^+(\eta, \eta) = -\frac{1}{4\pi\eta_2} + O(1)$.
- 3.1) If $\bar{\Gamma}(\bar{x}, \bar{z}) = \frac{\partial^2 \Gamma_0(\bar{x}, \bar{z})}{\partial \bar{z}_1^2}$, then $\omega^+(\eta, \eta) = -\frac{1}{8\pi\eta_2^2} + \frac{i\lambda(a)}{2\pi\eta_2} + O(1)$.
- 3.2) If $\bar{\Gamma}(\bar{x}, \bar{z}) = \frac{\partial^2 \Gamma_0(\bar{x}, \bar{z})}{\partial \bar{z}_1 \partial \bar{z}_2}$, then $\omega^+(\eta, \eta) = O(1)$.

We now evaluate the asymptotic behavior of $\tilde{\varphi}(\eta, \eta)$ using the asymptotic behavior of $\omega^+(\eta, \eta)$. Denoting by $\tilde{R}(\xi, \eta) = \tilde{\varphi}(\xi, \eta) - \omega^+(\xi, \eta)$, we have

$$\nabla \cdot [M \nabla \tilde{R}(\xi, \eta)] = \nabla \cdot [(I - M) \nabla \omega^+(\xi, \eta)], \quad \xi \in \tilde{D} \cap \mathbb{R}_+^2, \quad (39)$$

and it follows from the boundary conditions of (37) and (38) that for $\xi \in \partial \tilde{D} \cap \partial \mathbb{R}_+^2$, we have

$$\begin{aligned} & M \nabla \tilde{R}(\xi, \eta) \cdot \nu(\xi) + i\lambda(a) |J^T \nu(\xi)| \tilde{R}(\xi, \eta) \\ &= - [\nabla_{\bar{x}} \bar{\Gamma}(\Theta^{-1}(\xi), \Theta^{-1}(\eta)) \cdot J^T \nu(\xi) + i\lambda(a) |J^T \nu(\xi)| \bar{\Gamma}(\Theta^{-1}(\xi), \Theta^{-1}(\eta))] \\ &\quad - M \nabla \omega^+(\xi, \eta) \cdot \nu(\xi) - i\lambda(a) |J^T \nu(\xi)| \omega^+(\xi, \eta) \\ &= - [\nabla_{\bar{x}} \bar{\Gamma}(\Theta^{-1}(\xi), \Theta^{-1}(\eta)) \cdot J^T \nu(\xi) + i\lambda(a) |J^T \nu(\xi)| \bar{\Gamma}(\Theta^{-1}(\xi), \Theta^{-1}(\eta))] \\ &\quad + (I - M) \nabla \omega^+(\xi, \eta) \cdot \nu(\xi) + i\lambda(a) (1 - |J^T \nu(\xi)|) \omega^+(\xi, \eta) + \left[\frac{\partial}{\partial \nu} + i\lambda(a) \right] \bar{\Gamma}(\xi, \eta) \\ &= (I - M) \nabla \omega^+(\xi, \eta) \cdot \nu(\xi) + i\lambda(a) (1 - |J^T \nu(\xi)|) \omega^+(\xi, \eta) \\ &\quad + i\lambda(a) [\bar{\Gamma}(\xi, \eta) - |J^T \nu(\xi)| \bar{\Gamma}(\Theta^{-1}(\xi), \Theta^{-1}(\eta))] \\ &\quad + \frac{\partial \bar{\Gamma}(\xi, \eta)}{\partial \nu} - \nabla_{\bar{x}} \bar{\Gamma}(\Theta^{-1}(\xi), \Theta^{-1}(\eta)) \cdot J^T \nu(\xi). \end{aligned} \quad (40)$$

We will show in the following that the highest singularities of $\varphi(x, z)$ (or equivalently, $\tilde{\varphi}(\xi, \eta)$) shown in the theorem come from those of $\omega^+(\xi, \eta)$ while $\tilde{R}(\xi, \eta)$ contains the lower singularities. However, these lower singularities involve the geometrical properties and the surface impedance of ∂D . To evaluate $\tilde{R}(\xi, \eta)$, we make use of the Green's function in the upper half space which satisfies the problem

$$\begin{cases} \nabla \cdot [M\nabla G(\xi, \eta)] = -\delta(\xi - \eta), & \xi \in \mathbb{R}_+^2, \\ M\nabla G(\xi, \eta) \cdot \nu(\xi) + i\lambda(a)|J^T \nu(\xi)|G(\xi, \eta) = 0, & \xi \in \partial\mathbb{R}_+^2. \end{cases} \quad (41)$$

We now consider two fixed values $r_1, r_2 > 0$ such that the rectangle $Q = \{(\xi_1, \xi_2) : -r_1 + \eta_1 \leq \xi_1 \leq r_1 + \eta_1, 0 \leq \xi_2 \leq r_2\}$ lies totally in \tilde{D} (see Figure 1(b)). We denote by $S = \partial Q \cap \partial\mathbb{R}_+^2$ and $S^c = \partial Q \setminus S$. We recall that $\eta \in Q \cap C(0, \theta)$. Multiplying both sides of (39) by $G(\xi, \eta)$ and both sides of the first equation of (41) by $\tilde{R}(\xi, \eta)$, taking the difference and integrating it over Q , we obtain

$$\begin{aligned} & \int_Q \left\{ \nabla \cdot [M\nabla \tilde{R}(\xi, \eta)]G(\xi, \eta) - \nabla \cdot [M\nabla G(\xi, \eta)]\tilde{R}(\xi, \eta) \right\} d\xi \\ &= \int_Q \nabla \cdot [(I - M)\nabla \omega^+(\xi, \eta)]G(\xi, \eta) d\xi + \tilde{R}(\eta, \eta). \end{aligned}$$

Integrating by parts the first and the second integrals, we have

$$\begin{aligned} & \int_{\partial Q} M\nabla \tilde{R}(\xi, \eta) \cdot \nu G(\xi, \eta) ds(\xi) - \int_Q M\nabla \tilde{R}(\xi, \eta) \cdot \nabla G(\xi, \eta) d\xi \\ & - \int_{\partial Q} M\nabla G(\xi, \eta) \cdot \nu \tilde{R}(\xi, \eta) ds(\xi) + \int_Q M\nabla G(\xi, \eta) \cdot \nabla \tilde{R}(\xi, \eta) d\xi \\ &= \int_{\partial Q} (I - M)\nabla \omega^+(\xi, \eta) \cdot \nu G(\xi, \eta) ds(\xi) - \int_Q (I - M)\nabla \omega^+(\xi, \eta) \cdot \nabla G(\xi, \eta) d\xi + \tilde{R}(\eta, \eta). \end{aligned}$$

Since M is symmetric (see (36)), the second and the fourth terms on the left hand side cancel each other. Taking into account the boundary condition in (41), we obtain

$$\begin{aligned} \tilde{R}(\eta, \eta) &= \int_S M\nabla \tilde{R}(\xi, \eta) \cdot \nu G(\xi, \eta) ds(\xi) + i\lambda(a) \int_S |J^T \nu(\xi)| \tilde{R}(\xi, \eta) G(\xi, \eta) ds(\xi) \\ & + \int_{S^c} M\nabla \tilde{R}(\xi, \eta) \cdot \nu G(\xi, \eta) ds(\xi) - \int_{S^c} M\nabla G(\xi, \eta) \cdot \nu \tilde{R}(\xi, \eta) ds(\xi) \\ & - \int_S (I - M)\nabla \omega^+(\xi, \eta) \cdot \nu G(\xi, \eta) ds(\xi) - \int_{S^c} (I - M)\nabla \omega^+(\xi, \eta) \cdot \nu G(\xi, \eta) ds(\xi) \\ & + \int_Q (I - M)\nabla \omega^+(\xi, \eta) \cdot \nabla G(\xi, \eta) d\xi. \end{aligned} \quad (42)$$

Moreover, using the boundary condition (40) we obtain

$$\begin{aligned}
& \int_S M \nabla \tilde{R}(\xi, \eta) \cdot \nu G(\xi, \eta) ds(\xi) = -i\lambda(a) \int_S |J^T \nu(\xi)| \tilde{R}(\xi, \eta) G(\xi, \eta) ds(\xi) \\
& + \int_S (I - M) \nabla \omega^+(\xi, \eta) \cdot \nu(\xi) G(\xi, \eta) ds(\xi) + i\lambda(a) \int_S (1 - |J^T \nu(\xi)|) \omega^+(\xi, \eta) G(\xi, \eta) ds(\xi) \\
& + i\lambda(a) \int_S [\bar{\Gamma}(\xi, \eta) - |J^T \nu(\xi)| \bar{\Gamma}(\Theta^{-1}(\xi), \Theta^{-1}(\eta))] G(\xi, \eta) ds(\xi) \\
& + \int_S \left[\frac{\partial \bar{\Gamma}(\xi, \eta)}{\partial \nu} - \nabla_{\bar{x}} \bar{\Gamma}(\Theta^{-1}(\xi), \Theta^{-1}(\eta)) \cdot J^T \nu(\xi) \right] G(\xi, \eta) ds(\xi).
\end{aligned} \tag{43}$$

As will be shown in the following, the integrands in (42) are only singular at $\xi = \eta$ and $\xi = \eta^*$, where η^* is the image point of η over the ξ_1 -axis, i.e. $\eta^* = (\eta_1, -\eta_2)$ (see Figure 1(b)). Therefore, when $\eta \rightarrow 0$, say, $|\eta_1| < r_1/2, \eta_2 < r_2/2$, the integrals on S^c are bounded. From (42) and (43) we can represent $\tilde{R}(\eta, \eta)$ as follows

$$\begin{aligned}
\tilde{R}(\eta, \eta) &= i\lambda(a) \int_S (1 - |J^T \nu(\xi)|) \omega^+(\xi, \eta) G(\xi, \eta) ds(\xi) \\
&+ i\lambda(a) \int_S [\bar{\Gamma}(\xi, \eta) - |J^T \nu(\xi)| \bar{\Gamma}(\Theta^{-1}(\xi), \Theta^{-1}(\eta))] G(\xi, \eta) ds(\xi) \\
&+ \int_S \left[\frac{\partial \bar{\Gamma}(\xi, \eta)}{\partial \nu} - \nabla_{\bar{x}} \bar{\Gamma}(\Theta^{-1}(\xi), \Theta^{-1}(\eta)) \cdot J^T \nu(\xi) \right] G(\xi, \eta) ds(\xi) \\
&+ \int_Q (I - M) \nabla \omega^+(\xi, \eta) \cdot \nabla G(\xi, \eta) d\xi + O(1) \\
&= I_1 + I_2 + O(1),
\end{aligned} \tag{44}$$

where

$$\begin{aligned}
I_1 &= i\lambda(a) \int_S (1 - |J^T \nu(\xi)|) \omega^+(\xi, \eta) G(\xi, \eta) ds(\xi) \\
&+ i\lambda(a) \int_S [\bar{\Gamma}(\xi, \eta) - |J^T \nu(\xi)| \bar{\Gamma}(\Theta^{-1}(\xi), \Theta^{-1}(\eta))] G(\xi, \eta) ds(\xi) \\
&+ \int_Q (I - M) \nabla \omega^+(\xi, \eta) \cdot \nabla G(\xi, \eta) d\xi.
\end{aligned} \tag{45}$$

and

$$I_2 = \int_S \left[\frac{\partial \bar{\Gamma}(\xi, \eta)}{\partial \nu} - \nabla_{\bar{x}} \bar{\Gamma}(\Theta^{-1}(\xi), \Theta^{-1}(\eta)) \cdot J^T \nu(\xi) \right] G(\xi, \eta) ds(\xi), \tag{46}$$

The following lemmas show the asymptotic behaviors of the terms I_1 and I_2 . They also show that the former is more regular than the latter.

Lemma 3.5. *The integral I_1 is bounded for $\bar{\Gamma}(\bar{x}, \bar{z}) = \Gamma_0(\bar{x}, \bar{z})$ or $\bar{\Gamma}(\bar{x}, \bar{z}) = \frac{\partial}{\partial \bar{z}_j} \Gamma_0(\bar{x}, \bar{z})$, $j \in \{1, 2\}$, and for $\bar{\Gamma}(\bar{x}, \bar{z}) = \frac{\partial^2}{\partial \bar{z}_j \partial \bar{z}_l} \Gamma_0(\bar{x}, \bar{z})$, $j, l \in \{1, 2\}$, we have*

$$I_1 = O(\ln \eta_2) \text{ as } \tilde{D} \cap C(0, \theta) \ni \eta \rightarrow 0.$$

Lemma 3.6. *The integral I_2 is bounded for $\bar{\Gamma}(\bar{x}, \bar{z}) = \Gamma_0(\bar{x}, \bar{z})$ or $\bar{\Gamma}(\bar{x}, \bar{z}) = \frac{\partial}{\partial \bar{z}_j} \Gamma_0(\bar{x}, \bar{z})$, $j \in \{1, 2\}$. For $\bar{\Gamma}(\bar{x}, \bar{z}) = \frac{\partial^2}{\partial \bar{z}_1^2} \Gamma_0(\bar{x}, \bar{z})$ we have*

$$I_2 = \frac{f_a''(0)}{16\pi\eta_2} + O((\ln \eta_2)^2), \quad (47)$$

while for $\bar{\Gamma}(\bar{x}, \bar{z}) = \frac{\partial^2}{\partial \bar{z}_1 \partial \bar{z}_2} \Gamma_0(\bar{x}, \bar{z})$ we have

$$I_2 = -\frac{f_a''(0)\eta_1}{8\pi\eta_2^2} + O((\ln \eta_2)^2), \quad (48)$$

as $\tilde{D} \cap C(0, \theta) \ni \eta \rightarrow 0$.

The proofs of these two lemmas are similar to those of Lemmas 3.7 and 3.8 of our previous paper [15] for obstacles with Dirichlet boundary condition. Moreover, only the second term I_2 contains the singularities that play important roles in our analysis. Hence we only give the proof of Lemma 3.6 in the appendix. The proof of Lemma 3.5 is omitted.

Returning to the proof of Theorem 3.2, we can write $\tilde{\varphi}(\eta, \eta)$ as

$$\tilde{\varphi}(\eta, \eta) = \omega^+(\eta, \eta) + \tilde{R}(\eta, \eta) = \omega^+(\eta, \eta) + I_1 + I_2 + O(1).$$

From Lemmas 3.4, 3.5 and 3.6 we have the following cases:

1) $\bar{\Gamma}(\bar{x}, \bar{z}) = \Gamma_0(\bar{x}, \bar{z})$, then

$$\tilde{\varphi}(\eta, \eta) = \omega^+(\eta, \eta) + O(1) = -\frac{1}{2\pi} \ln \eta_2 + O(1). \quad (49)$$

2.1) $\bar{\Gamma}(\bar{x}, \bar{z}) = \frac{\partial}{\partial \bar{z}_1} \Gamma_0(\bar{x}, \bar{z})$, then

$$\tilde{\varphi}(\eta, \eta) = \omega^+(\eta, \eta) + O(1) = O(1). \quad (50)$$

2.2) $\bar{\Gamma}(\bar{x}, \bar{z}) = \frac{\partial}{\partial \bar{z}_2} \Gamma_0(\bar{x}, \bar{z})$, then

$$\tilde{\varphi}(\eta, \eta) = \omega^+(\eta, \eta) + O(1) = -\frac{1}{4\pi\eta_2} + O(1). \quad (51)$$

3.1) $\bar{\Gamma}(\bar{x}, \bar{z}) = \frac{\partial^2}{\partial \bar{z}_1^2} \Gamma_0(\bar{x}, \bar{z})$, then

$$\tilde{\varphi}(\eta, \eta) = \omega^+(\eta, \eta) + I_1 + I_2 + O(1) = -\frac{1}{8\pi\eta_2} + \frac{8i\lambda(a) + f_a''(0)}{16\pi\eta_2} + O((\ln \eta_2)^2). \quad (52)$$

3.2) $\bar{\Gamma}(\bar{x}, \bar{z}) = \frac{\partial^2}{\partial \bar{z}_1 \partial \bar{z}_2} \Gamma_0(\bar{x}, \bar{z})$, then

$$\tilde{\varphi}(\eta, \eta) = \omega^+(\eta, \eta) + I_1 + I_2 + O(1) = -\frac{f_a''(0)\eta_1}{16\pi\eta_2^2} + O((\ln \eta_2)^2). \quad (53)$$

We note that $\frac{\eta_1}{\eta_2} = \tan \theta_{z_a}$ and η_2 is of the same order as $|(z - a) \cdot \nu(a)|$. Then, Theorem 3.2 now follows from the equations (33), (49)–(53) and the superposition of the solutions of (32). The proof is complete. \square

3.2 On the blowup of the original indicator function

Since the order of the limits $\lim_{z \rightarrow a} \lim_{\delta \rightarrow 0} v_{g_{z, \alpha}^\delta}(z)$ cannot be interchangeable, we cannot derive a similar asymptotic expansion as theorem 3.2 for the original indicator function $v_{g_{z, \alpha}^\delta}(z)$, see [15]. However, using

our theorem 3.2, theorem 3.1 of [2] and some modifications of the proof of theorem 3.3 of [1] we can obtain a similar expansion of $v_{g_{z,\alpha}^\delta}(z)$ if the noise level is small enough. The analysis is given hereafter.

For an arbitrary positive scalar $h > 0$, we define the domain $D_h = \{x \in D : \text{dist}(x, \partial D) < h\}$, with $\text{dist}(x, \partial D)$ being the distance from x to ∂D . Consider the general interior problem

$$\begin{cases} \Delta w(x) + \kappa^2 w(x) = 0, & x \in D, \\ \left[\frac{\partial}{\partial \nu} + i\lambda(x) \right] w(x) = f(x), & x \in \partial D, \end{cases}$$

with $f \in H^{-1/2}(\partial D)$. Defining the impedance Green function $G(x, z)$ in D as the solution to the problem

$$\begin{cases} \Delta G(x, z) + \kappa^2 G(x, z) = -\delta(x - z), & x \in D, \\ \left[\frac{\partial}{\partial \nu} + i\lambda(x) \right] w(x) = 0, & x \in \partial D, \end{cases}$$

and using the Green second identity we obtain

$$w(z) = \int_{\partial D} G(x, z) f(x) ds(x), \quad z \in D.$$

Let us consider the point $z \in D_h$. From this equality we have

$$|w(z)| \leq \|G(\cdot, z)\|_{H^{1/2}(\partial D)} \|f\|_{H^{-1/2}(\partial D)}.$$

Note that $G(\cdot, z)$ does not belong to $H^1(D)$ due to the singularity at $x = z$. However, using the interpolation of $H^{1/2}(\partial D)$ in terms of $L^2(\partial D)$ and $H^1(\partial D)$ (see, e.g. [11], chapter 1) and the estimate $\|G(\cdot, z)\|_{H^1(\partial D)} \leq C^* h^{-1/2}$ with some positive constant C^* for $z \in D_h$ (see [16]), we have

$$|w(z)| \leq C h^{-1/2} \|f\|_{H^{-1/2}(\partial D)}$$

for some constant C . Now we replace $w(x)$ by $v_{g_{z,\alpha}^\delta}(x) - \varphi(x, z)$. In this case we have

$$f(x) = H g_{z,\alpha}^\delta(x) + \left[\frac{\partial}{\partial \nu} + i\lambda(x) \right] \psi(x, z), \quad x \in \partial D.$$

Substituting this function into the above inequality, we obtain

$$|v_{g_{z,\alpha}^\delta}(z) - \varphi(z, z)| \leq C h^{-1/2} \left\| H g_{z,\alpha}^\delta + \left[\frac{\partial}{\partial \nu} + i\lambda \right] \psi(\cdot, z) \right\|_{H^{-1/2}(\partial D)} \quad \text{for } z \in D_h. \quad (54)$$

To evaluate the right hand side of (54), we follow the same arguments as in the proof of theorem 3.1 of [2]. We obtain

$$\begin{aligned} \left\| H g_{z,\alpha}^\delta + \left[\frac{\partial}{\partial \nu} + i\lambda \right] \psi(\cdot, z) \right\|_{H^{-1/2}(\partial D)} &\leq \left\| H(\alpha I + F^* F)^{-1} F^* \psi^\infty(\cdot, z) + \left[\frac{\partial}{\partial \nu} + i\lambda \right] \psi(\cdot, z) \right\|_{H^{-1/2}(\partial D)} \\ &\quad + \|H\| \|\psi^\infty(\cdot, z)\|_{L^2(\mathbb{S}^1)} \left[\frac{\delta}{\alpha} + 2\|(F^\delta)^*\| \frac{\delta}{\alpha^{3/2}} \right]. \end{aligned} \quad (55)$$

The second term on the right hand side converges to zero as the noise level tends to zero if we choose α such that both $\frac{\delta}{\alpha}$ and $\frac{\delta}{\alpha^{3/2}}$ tend to zero [2]. Finally, we evaluate the first term on the right hand side of (55). To do so, we make use of similar arguments as in the proof of theorem 3.3 of [1], with $\left[\frac{\partial}{\partial \nu} + i\lambda \right] \psi(\cdot, z)$ (which plays the same role as the function φ in [1]) being replaced by $\left[\frac{\partial}{\partial \nu} + i\lambda \right] \psi(\cdot, z) \text{dist}^n(z, \partial D)$. Here the power n is chosen such that this function is bounded when z tends to ∂D . For example, if we consider the case of tripoles, then we can choose $n = 3$. Then using the arguments of [1], it follows that for every

$\epsilon > 0$, there exists some $\alpha^* = \alpha^*(h) > 0$ ¹, which is independent of z (since $[\frac{\partial}{\partial \nu} + i\lambda] \psi(\cdot, z) \text{dist}^n(z, \partial D)$ is uniformly bounded in D_h), such that for any $\alpha \leq \alpha^*$ we have

$$\left\| H(\alpha I + F^* F)^{-1} F^* \psi^\infty(\cdot, z) \text{dist}^n(z, \partial D) + \left[\frac{\partial}{\partial \nu} + i\lambda \right] \psi(\cdot, z) \text{dist}^n(z, \partial D) \right\|_{H^{-1/2}(\partial D)} < \epsilon.$$

Now for $z \in D_h$ we have

$$\left\| H(\alpha I + F^* F)^{-1} F^* \psi^\infty(\cdot, z) + \left[\frac{\partial}{\partial \nu} + i\lambda \right] \psi(\cdot, z) \right\|_{H^{-1/2}(\partial D)} < \frac{\epsilon}{h^n}. \quad (56)$$

It follows from (54)–(56) that

$$|v_{g_{z,\alpha}^\delta}(z) - \varphi(z, z)| \leq Ch^{-1/2} \left\{ \frac{\epsilon}{h^n} + \|H\| \|\psi^\infty(\cdot, z)\|_{L^2(\mathbb{S}^1)} \left[\frac{\delta}{\alpha} + 2\|(F^\delta)^*\| \frac{\delta}{\alpha^{3/2}} \right] \right\} \text{ for } z \in D_h. \quad (57)$$

Choose $\epsilon = h^{n+1}$, then the right hand side of (57) can be written as $O(h^{1/2} + \frac{\delta}{\alpha h^{1/2}} + \frac{\delta}{\alpha^{3/2} h^{1/2}})$.

We note that the condition that the second term on the right hand side of (57) converges to zero (as the noise level δ tends to zero) requires that the regularization parameter α should not be too small (compared to δ), say, $\alpha \geq \max\{\delta, \delta^{2/3}\}$. This condition may contradict the inequality $\alpha \leq \alpha^*$ for a given noise level because α^* can be too small. However, for the given α^* , there exists some $\delta^* := \delta^*(h) > 0$ such that for $\delta < \delta^*$, the regularization parameter α satisfies both conditions. Summarizing the above analysis we can interpret the result given in (57) in the following theorem.

Theorem 3.7. *For any given small $h > 0$, there exists some $\delta^* := \delta^*(h) > 0$ such that for $\delta \leq \delta^*$ we can choose the regularization parameter α satisfying $\alpha \leq \alpha^*(h)$ and $\frac{\delta}{\alpha h^{1/2}} + \frac{\delta}{\alpha^{3/2} h^{1/2}} \leq h^{1/2}$. Consequently, the blowup rate of the original indicator function $v_{g_{z,\alpha}^\delta}(z)$ is of the same order as its limit $\varphi(z, z)$ for $z \in D_h$. More precisely,*

$$v_{g_{z,\alpha}^\delta}(z) = \varphi(z, z) + O(h^{1/2}) \text{ for } z \in D_h. \quad (58)$$

4 Effect of the anisotropy of the background medium

In this section, we consider an obstacle placed in an anisotropic medium and analyze the role of the anisotropy on the asymptotic expansion of the limit of the indicator function. We first define briefly the forward and inverse scattering problems in the anisotropic medium. For a detailed consideration, we refer the reader to [7] for the 3D case. In our analysis, however, we confine to the 2D problem as in the isotropic medium.

For the anisotropic medium, the Helmholtz equation (1) is replaced by the equation

$$\nabla \cdot [A \nabla u_A^s(x)] + \kappa^2 u_A^s(x) = 0, \quad x \in \mathbb{R}^2 \setminus \bar{D}, \quad (59)$$

and the boundary condition (2) is replaced by

$$\left[\frac{\partial}{\partial \nu_A} + i\lambda(x) \right] [u_A^s(x) + u_A^i(x)] = 0, \quad x \in \partial D, \quad (60)$$

where A is a symmetric positive definite matrix which represents the anisotropy of the medium, $\nu_A = \nu \cdot A$ and the incident plane wave in the anisotropic medium is given by $u_A^i(x) = e^{ikA^{-1/2}x \cdot d}$. Note that the incident plane wave in the anisotropic medium propagates in the direction $A^{-1/2}d/|A^{-1/2}d|$ instead of the direction d .

¹ α^* is the upper bound of the regularization paramter in the noise-free case as used in [1].

The radiation condition is given as follows

$$d_A(x)\hat{x} \cdot A\nabla u_A^s(x) - i\kappa u_A^s(x) = O(r^{-3/2}), \quad r = |x| \rightarrow \infty, \quad (61)$$

where $d_A(x) := (x \cdot A^{-1}x)^{1/2}$. The far field pattern in this anisotropic medium is given by

$$u_A^\infty(\hat{x}, d) = \frac{e^{i\pi/4}}{\sqrt{8\pi\kappa \det A}} \int_{\partial D} \nu(y) \cdot \left[\hat{x} u_A^s(y) \frac{i\kappa}{d_A(\hat{x})} + A\nabla_y u_A^s(y) \right] \exp \left\{ -\frac{i\kappa(\hat{x} \cdot A^{-1}y)}{d_A(\hat{x})} \right\} ds(y) \quad (62)$$

As in the isotropic medium, the forward scattering problem is to find the scattered wave u_A^s from (59)–(61) given the incident wave u_A^i . The inverse problem is to reconstruct the shape D given the measured far field pattern $u_A^\infty(\hat{x}, d)$ for all $\hat{x}, d \in \mathbb{S}^1$.

Using the coordinate transformation $\tilde{x} = A^{-1/2}x$, denoting by \tilde{D} the obstacle in the \tilde{x} -coordinate system and $\tilde{u}^s(\tilde{x}) = u_A^s(x)$, problem (59)–(61) can be transformed into the same system as (1)–(3) but in the \tilde{x} -coordinate system for the obstacle \tilde{D}

$$\begin{cases} \Delta \tilde{u}^s(\tilde{x}) + \kappa^2 \tilde{u}^s(\tilde{x}) = 0, & \tilde{x} \in \mathbb{R}^2 \setminus \tilde{D}, \\ \left[\frac{\partial}{\partial \tilde{\nu}} + i\tilde{\lambda}(\tilde{x}) \right] [\tilde{u}^s(\tilde{x}) + \tilde{u}^i(\tilde{x})] = 0, & \tilde{x} \in \partial \tilde{D}, \\ \frac{\partial \tilde{u}^s(\tilde{x})}{\partial \tilde{r}} - i\kappa \tilde{u}^s(\tilde{x}) = O(\tilde{r}^{-3/2}), & \tilde{r} = |\tilde{x}|, \end{cases} \quad (63)$$

Similarly, the far field pattern (62) is transformed into the far field pattern of the isotropic problem.

From the above analysis, it is clear that all theoretical results (e.g. the well-posedness of the forward problem, the uniqueness of the inverse problems, etc.) for the transformed domain \tilde{D} in the isotropic medium can be carried over to the anisotropic problem. To solve the inverse problem of reconstructing the domain D from measured far field pattern, we first transform it into the isotropic problem and solve it by the LSM. After that, we transform the reconstructed domain into the anisotropic medium.

To analyze the effect of the anisotropy on the accuracy of the LSM, we first make use of the accuracy analysis presented in the previous section for the obstacle \tilde{D} in the isotropic medium. Then, transforming back into the x -coordinate system, we have the following asymptotic expansion of the limit of the indicator function, which we denote by φ_A , in the anisotropic medium using the combination of the tripoles (see (25))

$$\varphi_A(z, z) = \left[\frac{1}{64\pi^2 |hA^{1/2}\nu(a)|^4} - \frac{\mathcal{F}(i\lambda(a), f_a''(0), A)}{64\pi^2 |hA^{1/2}\nu(a)|^3} + O\left(\frac{1}{|hA^{1/2}\nu(a)|^2}\right) \right]^{1/2} \quad (64)$$

for z tends to $a \in \partial D$ in the normal direction, i.e., $z = a - h\nu(a)$. Here \mathcal{F} is a bounded function of its variables. We should emphasize that the normal vector $\nu(a)$ in the anisotropic medium may not be in the same direction as $\nu(\tilde{a})$ in the corresponding isotropic medium. Therefore, the third terms on the right hand side of (23) and (24) are still present and $\mathcal{F}(i\lambda(a), f_a''(0), A)$ takes into account all the first-order singular terms of (23) and (24).

It is clear from this asymptotic expansion that the blowup rate of the limit of the indicator function depends on not only the geometry and the impedance but also the anisotropy of the medium. Indeed, the value $|A^{1/2}\nu(a)|$ depends on the direction of the normal vector $\nu(a)$ at the point a . As a consequence, the blowup of $\varphi_a(z, z)$ varies along the obstacle boundary. Moreover, unlike the first two parameters, the anisotropy influences also the highest singular term of the asymptotic expansion. That means, its effect is even more visible than the first two parameters.

In the next section we illustrate this effect with some numerical examples.

5 Numerical results

In this section, we first present some numerical examples showing the effect of the curvature and the impedance of the obstacle boundary on the accuracy of the LSM. Then we show some results about

improving or deteriorating the accuracy.

In numerical implementation, the boundary of the obstacle is determined by drawing level curves of the indicator function. Theorem 3.2 shows the dependence of the blowup rate of (the limit of) the indicator function on the curvature and the impedance. That means, the similarity between the level curves and the true shape may depend on the variation of these parameters. To verify this phenomenon numerically, we consider two obstacles. The first one is the circle $\{x = 1.5(\cos t, \sin t), t \in [0, 2\pi)\}$ and the second one is the kite $\{x(t) = (\cos t + 0.65(\cos 2t - 1), \sin t), t \in [0, 2\pi)\}$.

In this paper, the measured far field pattern $u^\infty(\cdot, d)$ is simulated as the solution of the forward problem (1)–(3) which is solved by the integral equation method [6, 10]. In the next examples, the wave number is fixed at $\kappa = 2$. The number of incident directions is chosen to be 64. They are uniformly distributed on the unit circle. The observation directions are identical to the incident ones. The sampling area is chosen to be the square $[-3, 3]^2$ with the sampling grid of 0.05 in each direction. A random noise of 1% is added to the simulated far field pattern.

As we showed in our previous paper [15], the Herglotz wavefunction $v_{g_{z,\alpha}^\delta}$ usually provides more accurate reconstructions compared to its density $g_{z,\alpha}^\delta$, especially for multipoles. Therefore, in this paper we only consider the Herglotz wavefunction as the indicator function. Moreover, since the numerical solution to (14) and the associated Herglotz wavefunction are large in the exterior of the obstacle, we use the following normalized indicator function for better visualization [15]

$$\mathbb{I}(z) := [|v_{g_{z,\alpha}^\delta}(z)| + 1]^{-1}. \quad (65)$$

Level curves of the indicator functions are defined as the set of all sampling points satisfying

$$m + (n - 1) \frac{M - m}{N} \leq \mathbb{I}(z) < m + n \frac{M - m}{N},$$

for each $n = 1, 2, \dots, N$, where $m = \min_z \mathbb{I}(z)$ and $M = \max_z \mathbb{I}(z)$ and N is a positive integer determining the number of subintervals that the interval $[m, M]$ is divided into. In this section, the interval $[m, M]$ is divided into 100 subintervals, i.e., $N = 100$.

Our results in [15] also showed that using the multipoles as the right hand side of the far field equation (14) seems to provide more accurate results than the monopole. Therefore, in the following, we only show the results of tripoles.

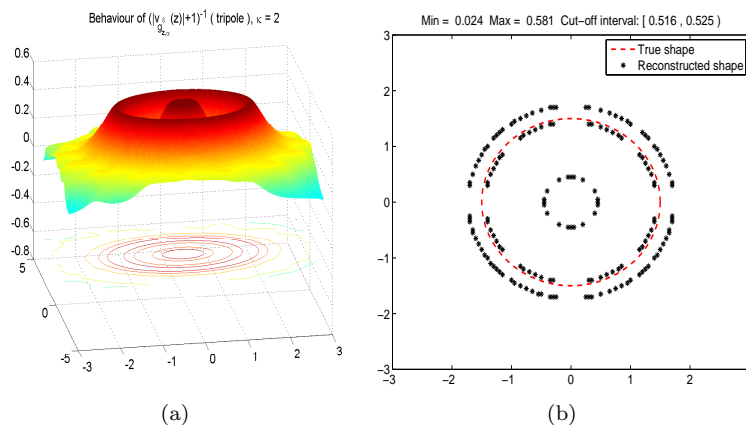


Figure 2: Reconstruction of the circle using tripoles for $\lambda(a) = -4i$: (a) The 3D view of the indicator function; (b) Level curves. The dash curve represents the true shape.

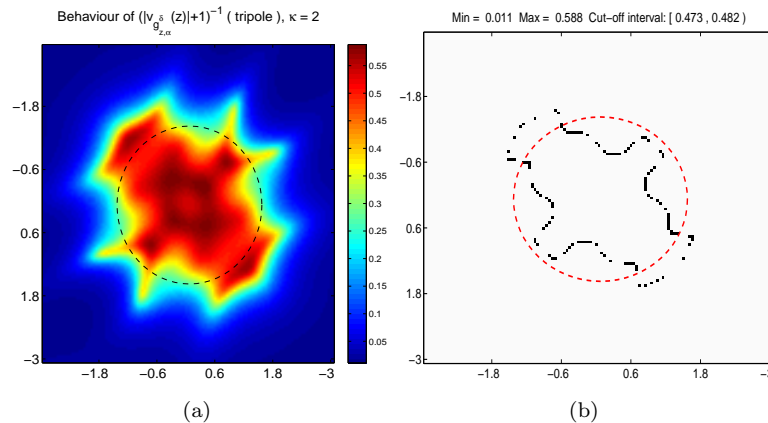


Figure 3: Reconstruction of the circle using tripoles for $\lambda(a(t)) = -4i \sin(2t)$: (a) The indicator function; (b) A level curve. The dash curve represents the true shape.

Effect of the curvature

We first show the effect of the curvature on the numerical accuracy of the LSM. For this purpose, we choose a constant impedance $\lambda(a) = -4i$, $a \in \partial D$.

The numerical indicator function for the circle in the case of tripoles and some level curves are depicted in Figure 2. Note that "the best" level curve overlaps the circle, we show these level curves for better visualization. Of course the accuracy of the LSM depends on the choice of the level curves, but we do not analyze this choice here. Instead, we choose a suitable level curve for each obstacle because our objective is to compare the accuracy on different parts, with possibly different curvature's values, of the boundary of each obstacle. The result for the kite is depicted in Figure 4.

Comparing these two figures we see clearly that the circle, with uniform curvature, is reconstructed with a very high accuracy but the reconstruction of the kite is reasonable in some parts and not good in other parts. Note that the curvature of the kite is not uniform, especially, it has two peaks at the two corners and is negative in the concave part of the obstacle. These results agree with theorem 3.2 (up to the effect of the log-type terms) since the second term on the right hand side of (23) and (24) (or (25)) is uniform on ∂D for the circle but not for the kite.

Effect of the impedance and coating

The effect of the impedance can be considered in two directions: destroying or improving the reconstruction accuracy. Let us first consider the destroying effect. To show the destruction of the accuracy, we consider the circle again with the impedance given by $\lambda(a(t)) = -4i \sin(2t)$, $t \in [0, 2\pi)$. It is clear that the asymptotic expansion (25) is not uniform anymore. The reconstruction of the circle is depicted in Figure 3.

The figure shows clearly that the reconstruction is destroyed due to the oscillatory behavior of the impedance. Comparing with Figure 2 we can see the destroying effect of the impedance. Therefore, in design problems, in order to deteriorate the reconstruction, we should coat the obstacle with a material of highly oscillatory impedance.

On the other hand, in order to improve the accuracy, we consider the kite and choose the impedance in such a way that it dominates the curvature as shown in (23) and (24). These asymptotic expansions suggest that we can choose the impedance either to dominate the curvature or to cancel the curvature in the first order singular term. Figure 5 shows the indicator function for the constant impedance $\lambda(a) = -15i =: \lambda_1(a)$, while Figure 6 shows the result for $\lambda(a) = -4i - f_a''(0)/8i =: \lambda_2(a)$, which cancels

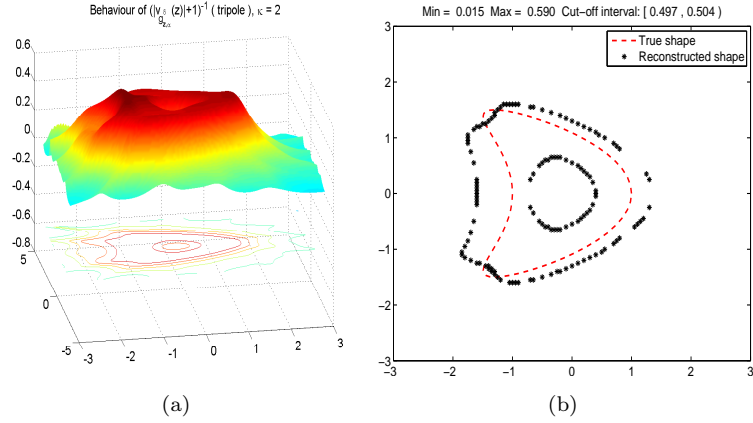


Figure 4: Reconstruction of the kite using tripoles for $\lambda(a) = -4i$: (a) The 3D view of the indicator function; (b) A level curve. The dash curve represents the true shape.

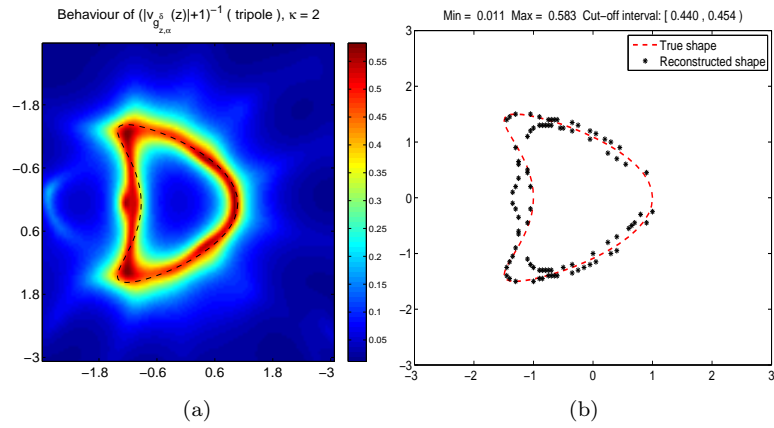


Figure 5: Reconstruction of the kite using tripoles with $\lambda(a) = -15i$: (a) The indicator function; (b) A level curve.

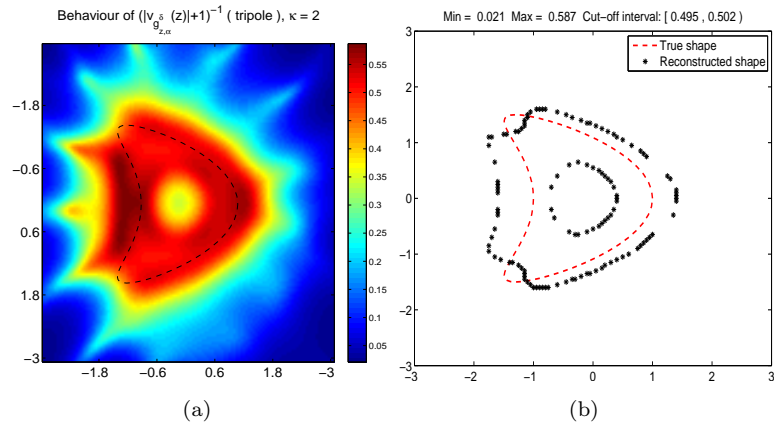


Figure 6: Reconstruction of the kite using tripoles with $\lambda(a) = -4i - f''_a(0)/8i$: (a) The indicator function; (b) A level curve.

the first order singular term in the asymptotic expansions (23) and (24).

Figure 5 shows that for the large constant impedance, $\lambda(a) = \lambda_1(a)$, the reconstruction is much better than the previous case (Figure 4). Unfortunately, as shown in Figure 6, the accuracy in the case of $\lambda(a) = \lambda_2(a)$ is not really improved even when the first singular term in the asymptotic expansions (23)–(24) is eliminated. The possible reason for this phenomenon is that the lower order terms of the asymptotic expansions may contain the derivatives of the impedance. For this reason, in the case of the large constant impedance, the effect of the lower order terms is small as all derivatives of the impedance are zero. Moreover, the curvature $f_a''(0)$ in the first order singular term is dominated by the large value of the impedance. For the case of $\lambda(a) = \lambda_2(a)$, although the first order singular term is eliminated, the lower order terms are more variant due to the variation of the derivatives of the impedance as a result of the variant curvature of the obstacle boundary.

This analysis suggests that in order to improve the reconstruction in design problems, we should cover the obstacle by a material of large, but constant, impedance.

Effect of the anisotropy of the medium

To see the effect of the anisotropy of the medium on the accuracy of the LSM, we consider two obstacles: the above circle $x = 1.5(\cos t, \sin t)$, $t \in [0, 2\pi)$ and the ellipse $x = (\cos t, 5 \sin t)$, $t \in [0, 2\pi)$, in the medium with the anisotropy matrix

$$A = \begin{pmatrix} 1 & 0 \\ 0 & 25 \end{pmatrix}$$

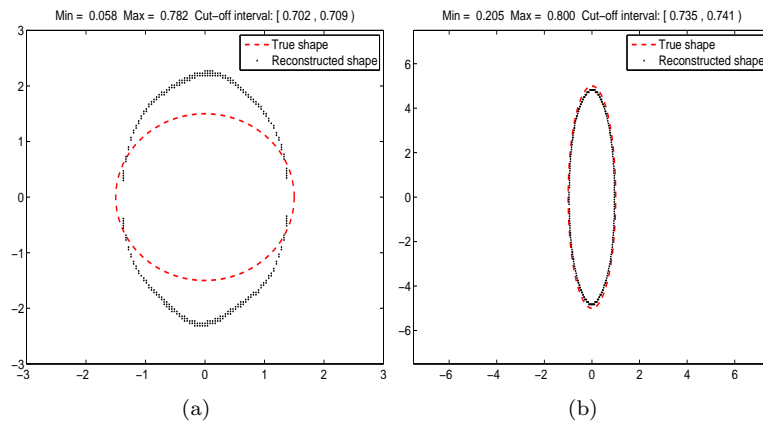


Figure 7: The effect of the anisotropic medium: (a) The circle; (b) The ellipse. The dash curve represents the true shape.

The reconstructions of the obstacles are depicted in Figure 7. Unlike in the isotropic medium, the circle is not accurately reconstructed. However, the reconstruction of the ellipse is very accurate. We note that this is "the best" ellipse with respect to the above anisotropic matrix. Indeed, if we consider the transformed problem in the \tilde{x} -coordinate system, this ellipse is transformed into a circle. However, the circle is transformed into an ellipse, which makes the reconstruction less accurate due to its non-uniform curvature. These examples confirm the effect of the anisotropy of the medium on the accuracy of the LSM as theoretically depicted in section 4.

6 Conclusions

We have shown the effect of the geometry and the impedance of an obstacle as well as the anisotropy of the background medium on the accuracy of the LSM. The theoretical results have shown that the blowup rate of the limit (as the noise level tends to zero) of the indicator function of the LSM depends on these parameters. A similar behavior is also true for the original indicator function for small enough noise level. These results were confirmed by numerical examples. Moreover, we have also proposed surface coating procedures for improving or destroying the accuracy in design problems. Our analysis suggested that to improve the accuracy, the impedance should be chosen to be large but constant. On the other hands, to destroy the accuracy, the impedance should be chosen to be highly oscillatory.

Acknowledgements

This work was supported by the Johann Radon Institute for Computational and Applied Mathematics (RICAM), Austrian Academy of Sciences.

7 Appendix: Proof of Lemma 3.6

To prove Lemma 3.6, we need the asymptotic expansion of the first derivatives of the Neumann Green's function $G(\xi, \eta)$ given in (41), see [15] for a similar result for the Dirichlet Green's function.

Lemma 7.1. *The first derivatives of the Green's function $G(\xi, \eta)$ for $\xi, \eta \in Q$ close enough to the origin can be written as follows*

$$\begin{aligned} G_{\xi_1} &:= \frac{\partial G}{\partial \xi_1} = -\frac{1}{2\pi} \left[\frac{\xi_1 - \eta_1}{|\xi - \eta|^2} + \frac{\xi_1 - \eta_1}{|\xi - \eta^*|^2} \right] + \frac{O(\eta_1)}{|\xi - \eta|} + O(\ln \eta_2), \quad |\xi - \eta| \rightarrow 0, \\ G_{\xi_2} &:= \frac{\partial G}{\partial \xi_2} = -\frac{1}{2\pi} \left[\frac{\xi_2 - \eta_2}{|\xi - \eta|^2} + \frac{\xi_2 + \eta_2}{|\xi - \eta^*|^2} \right] + \frac{O(\eta_1)}{|\xi - \eta|} + O(\ln \eta_2), \quad |\xi - \eta| \rightarrow 0. \end{aligned} \quad (66)$$

We only carry out the detail proof of Lemma 3.6 for the case 3.1, the other cases are similar. Using the representation (35) of the Jacobian J , we can rewrite the term I_2 of (46) in the form

$$I_2 = \int_{-r_1+\eta_1}^{r_1+\eta_1} \left\{ \frac{\partial \bar{\Gamma}}{\partial \bar{x}_2}(\Theta^{-1}(\xi), \Theta^{-1}(\eta)) - f'_a(\xi_1) \frac{\partial \bar{\Gamma}}{\partial \bar{x}_1}(\Theta^{-1}(\xi), \Theta^{-1}(\eta)) - \frac{\partial \bar{\Gamma}}{\partial \bar{x}_2}(\xi, \eta) \right\} G(\xi, \eta) d\xi_1. \quad (67)$$

To evaluate this integral, we make use of the explicit formulas of $\frac{\partial \bar{\Gamma}}{\partial \bar{x}_j}$, $j \in \{1, 2\}$. We have

$$\bar{\Gamma}(\bar{x}, \bar{z}) = \frac{\partial^2 \Gamma_0(\bar{x}, \bar{z})}{\partial \bar{z}_1^2} = \frac{1}{2\pi} \frac{(\bar{x}_1 - \bar{z}_1)^2 - (\bar{x}_2 - \bar{z}_2)^2}{|\bar{x} - \bar{z}|^4}.$$

Therefore,

$$\begin{aligned} \frac{\partial \bar{\Gamma}(\bar{x}, \bar{z})}{\partial \bar{x}_1} &= \frac{1}{\pi} \frac{(\bar{x}_1 - \bar{z}_1)[3(\bar{x}_2 - \bar{z}_2)^2 - (\bar{x}_1 - \bar{z}_1)^2]}{|\bar{x} - \bar{z}|^6}, \\ \frac{\partial \bar{\Gamma}(\bar{x}, \bar{z})}{\partial \bar{x}_2} &= \frac{1}{\pi} \frac{(\bar{x}_2 - \bar{z}_2)[(\bar{x}_2 - \bar{z}_2)^2 - 3(\bar{x}_1 - \bar{z}_1)^2]}{|\bar{x} - \bar{z}|^6}. \end{aligned} \quad (68)$$

We note that for $\xi \in S$, we have $\xi_2 = 0$. Hence, $\Theta^{-1}(\xi) = (\xi_1, f_a(\xi_1))^T$ and $\Theta^{-1}(\eta) = (\eta_1, \eta_2 + f_a(\eta_1))^T$. We first evaluate the term $|\Theta^{-1}(\xi) - \Theta^{-1}(\eta)|^{-6}$ which appears in the derivatives of $\bar{\Gamma}$. We have

$$\begin{aligned} |\Theta^{-1}(\xi) - \Theta^{-1}(\eta)|^2 &= (\xi_1 - \eta_1)^2 + [f_a(\xi_1) - f_a(\eta_1) - \eta_2]^2 \\ &= |\xi - \eta|^2 - 2\eta_2[f_a(\xi_1) - f_a(\eta_1)] + [f_a(\xi_1) - f_a(\eta_1)]^2. \end{aligned}$$

On the other hand, using the Taylor expansion, we have

$$f_a(\xi_1) - f_a(\eta_1) = f'_a(\eta_1)(\xi_1 - \eta_1) + \frac{1}{2}f''_a(\eta_1)(\xi_1 - \eta_1)^2 + O((\xi_1 - \eta_1)^3). \quad (69)$$

Here we have used the Lipschitz condition for the second derivative of f_a . Hence,

$$\begin{aligned} |\Theta^{-1}(\xi) - \Theta^{-1}(\eta)|^2 &= |\xi - \eta|^2 \left\{ 1 - 2\eta_2 f'_a(\eta_1) \frac{\xi_1 - \eta_1}{|\xi - \eta|^2} - \eta_2 f''_a(\eta_1) \frac{(\xi_1 - \eta_1)^2}{|\xi - \eta|^2} \right. \\ &\quad \left. + [f'_a(\eta_1)]^2 \frac{(\xi_1 - \eta_1)^2}{|\xi - \eta|^2} + f'_a(\eta_1) f''_a(\eta_1) \frac{(\xi_1 - \eta_1)^3}{|\xi - \eta|^2} + O((\xi_1 - \eta_1)^2) \right\}. \end{aligned}$$

We note that $f'(\eta_1) = O(\eta_1) \rightarrow 0$ as η tends to the origin, which is the case under consideration in this analysis. Hence we can assume that when ξ is close enough to η , the absolute value of the sum of the last five terms on the right hand side is less than 1. Using the equality

$$\frac{1}{1+x} = 1 - x + x^2 - \dots$$

for $|x| < 1$, we obtain

$$\begin{aligned} \frac{1}{|\Theta^{-1}(\xi) - \Theta^{-1}(\eta)|^2} &= \frac{1}{|\xi - \eta|^2} \left\{ 1 + 2\eta_2 f'_a(\eta_1) \frac{\xi_1 - \eta_1}{|\xi - \eta|^2} + \eta_2 f''_a(\eta_1) \frac{(\xi_1 - \eta_1)^2}{|\xi - \eta|^2} \right. \\ &\quad \left. + [f'_a(\eta_1)]^2 O(1) + f'_a(\eta_1) O(\xi_1 - \eta_1) + O((\xi_1 - \eta_1)^2) \right\}. \end{aligned}$$

For the simplicity of analysis, we also make use of the estimate $f'(\eta_1) = O(\eta_2) = O(|\xi - \eta|)$. From this and the above equality we have

$$\frac{1}{|\Theta^{-1}(\xi) - \Theta^{-1}(\eta)|^6} = \frac{1}{|\xi - \eta|^6} \left\{ 1 + 6\eta_2 f'_a(\eta_1) \frac{\xi_1 - \eta_1}{|\xi - \eta|^2} + 3\eta_2 f''_a(\eta_1) \frac{(\xi_1 - \eta_1)^2}{|\xi - \eta|^2} + O(|\xi - \eta|^2) \right\}. \quad (70)$$

Using the Taylor expansion (69) again, we can also write $f_a(\xi_1) - f_a(\eta_1) = O(|\xi - \eta|^2)$ for $\xi \in S$. Replacing this equality, (69) and (70) into (68), we obtain

$$\begin{aligned} \frac{\partial \bar{\Gamma}}{\partial \bar{x}_2}(\Theta^{-1}(\xi), \Theta^{-1}(\eta)) &= \frac{1}{\pi} \frac{[f_a(\xi_1) - \eta_2 - f_a(\eta_1)]\{[f_a(\xi_1) - \eta_2 - f_a(\eta_1)]^2 - 3(\xi_1 - \eta_1)^2\}}{|\Theta^{-1}(\xi) - \Theta^{-1}(\eta)|^6} \\ &= \frac{1}{\pi |\xi - \eta|^6} \left\{ 1 + 6\eta_2 f'_a(\eta_1) \frac{\xi_1 - \eta_1}{|\xi - \eta|^2} + 3\eta_2 f''_a(\eta_1) \frac{(\xi_1 - \eta_1)^2}{|\xi - \eta|^2} + O(|\xi - \eta|^2) \right\} \\ &\times \left\{ O(|\xi - \eta|^5) + 3[\eta_2^2 - (\xi_1 - \eta_1)^2][f'_a(\eta_1)(\xi_1 - \eta_1) + \frac{1}{2}f''_a(\eta_1)(\xi_1 - \eta_1)^2] - \eta_2[\eta_2^2 - 3(\xi_1 - \eta_1)^2] \right\} \quad (71) \\ &= \frac{\partial \bar{\Gamma}}{\partial \bar{x}_2}(\xi, \eta) + \frac{3f'_a(\eta_1)}{\pi |\xi - \eta|^6} (\xi_1 - \eta_1) \left[\eta_2^2 - (\xi_1 - \eta_1)^2 - 2\eta_2^2 \frac{\eta_2^2 - 3(\xi_1 - \eta_1)^2}{|\xi - \eta|^2} \right] \\ &+ \frac{3f''_a(\eta_1)}{2\pi |\xi - \eta|^6} (\xi_1 - \eta_1)^2 \left[\eta_2^2 - (\xi_1 - \eta_1)^2 - 2\eta_2^2 \frac{\eta_2^2 - 3(\xi_1 - \eta_1)^2}{|\xi - \eta|^2} \right] + \frac{O(1)}{|\xi - \eta|}. \end{aligned}$$

Similarly,

$$\begin{aligned} \frac{\partial \bar{\Gamma}}{\partial \bar{x}_1}(\Theta^{-1}(\xi), \Theta^{-1}(\eta)) &= \frac{1}{\pi} \frac{(\xi_1 - \eta_1)\{3[f_a(\xi_1) - \eta_2 - f_a(\eta_1)]^2 - (\xi_1 - \eta_1)^2\}}{|\Theta^{-1}(\xi) - \Theta^{-1}(\eta)|^6} \\ &= \frac{\xi_1 - \eta_1}{\pi |\xi - \eta|^6} \left[1 + 6\eta_2 f'_a(\eta_1) \frac{\xi_1 - \eta_1}{|\xi - \eta|^2} + 3\eta_2 f''_a(\eta_1) \frac{(\xi_1 - \eta_1)^2}{|\xi - \eta|^2} + O(|\xi - \eta|^2) \right] \\ &\times \{O(|\xi - \eta|^3) + 3\eta_2^2 - (\xi_1 - \eta_1)^2\} \\ &= \frac{\xi_1 - \eta_1}{\pi |\xi - \eta|^6} [3\eta_2^2 - (\xi_1 - \eta_1)^2 + O(|\xi - \eta|^3)]. \end{aligned}$$

In this analysis, we also make use of the expansion

$$f'_a(\xi_1) = f'_a(\eta_1) + f''_a(\eta_1)(\xi_1 - \eta_1) + O((\xi_1 - \eta_1)^2).$$

From these two equalities we arrive at

$$\begin{aligned} f'_a(\xi_1) \frac{\partial \bar{\Gamma}}{\partial \bar{x}_1}(\Theta^{-1}(\xi), \Theta^{-1}(\eta)) &= \frac{f'_a(\eta_1)}{\pi|\xi - \eta|^6} (\xi_1 - \eta_1) [3\eta_2^2 - (\xi_1 - \eta_1)^2] \\ &+ \frac{f''_a(\eta_1)}{\pi|\xi - \eta|^6} (\xi_1 - \eta_1)^2 [3\eta_2^2 - (\xi_1 - \eta_1)^2] + \frac{O(1)}{|\xi - \eta|}. \end{aligned} \quad (72)$$

Replacing (71) and (72) into (67), after some direct calculations, with the notation $\bar{\xi}_1 = \xi_1 - \eta_1$, we have

$$\begin{aligned} I_2 &= -\frac{2f'_a(\eta_1)}{\pi} \int_{-r_1}^{r_1} \frac{\bar{\xi}_1 [3\eta_2^4 - 8\eta_2^2 \bar{\xi}_1^2 + \bar{\xi}_1^4]}{(\bar{\xi}_1^2 + \eta_1^2)^4} G(\xi, \eta) d\bar{\xi}_1 \\ &- \frac{f''_a(\eta_1)}{2\pi} \int_{-r_1}^{r_1} \frac{\bar{\xi}_1^2 [9\eta_2^4 - 14\eta_2^2 \bar{\xi}_1^2 + \bar{\xi}_1^4]}{(\bar{\xi}_1^2 + \eta_1^2)^4} G(\xi, \eta) d\bar{\xi}_1 + \int_{-r_1}^{r_1} \frac{O(1)}{|\xi - \eta|} G(\xi, \eta) d\bar{\xi}_1. \end{aligned} \quad (73)$$

From Lemma 7.1 it is clear that the last integral is of the order $O((\ln \eta_2)^2)$. We show that the first integral is bounded. Indeed, we first have

$$\int_{-r_1}^{r_1} \frac{\bar{\xi}_1 [3\eta_2^4 - 8\eta_2^2 \bar{\xi}_1^2 + \bar{\xi}_1^4]}{(\bar{\xi}_1^2 + \eta_1^2)^4} \left[\frac{1}{2\pi} \ln \frac{1}{|\xi - \eta|} + C \right] d\bar{\xi}_1 = 0$$

because the integrand is an odd function of $\bar{\xi}_1$. Moreover,

$$\begin{aligned} &f'_a(\eta_1) \int_{-r_1}^{r_1} \frac{\bar{\xi}_1 [3\eta_2^4 - 8\eta_2^2 \bar{\xi}_1^2 + \bar{\xi}_1^4]}{(\bar{\xi}_1^2 + \eta_1^2)^4} O(|\xi - \eta|) d\bar{\xi}_1 \\ &= f'_a(\eta_1) \int_{-r_1}^{r_1} \frac{O(1)}{(\bar{\xi}_1^2 + \eta_2^2)^{1/2}} d\bar{\xi}_1 = \frac{f'_a(\eta_1) O(1)}{\eta_2} = O(1). \end{aligned}$$

To evaluate the second integral of (73), we make use of integration by parts. We have

$$\begin{aligned} &\int_{-r_1}^{r_1} \frac{\bar{\xi}_1^2 [9\eta_2^4 - 14\eta_2^2 \bar{\xi}_1^2 + \bar{\xi}_1^4]}{(\bar{\xi}_1^2 + \eta_1^2)^4} G(\xi, \eta) d\bar{\xi}_1 \\ &= \left[\frac{5\eta_2^2 \bar{\xi}_1}{(\eta_2^2 + \bar{\xi}_1^2)^2} - \frac{\bar{\xi}_1}{\eta_2^2 + \bar{\xi}_1^2} - \frac{4\eta_2^4 \bar{\xi}_1}{(\eta_2^2 + \bar{\xi}_1^2)^3} \right] G(\xi, \eta) \Big|_{-r_1}^{r_1} \\ &- \int_{-r_1}^{r_1} \left[\frac{5\eta_2^2 \bar{\xi}_1}{(\eta_2^2 + \bar{\xi}_1^2)^2} - \frac{\bar{\xi}_1}{\eta_2^2 + \bar{\xi}_1^2} - \frac{4\eta_2^4 \bar{\xi}_1}{(\eta_2^2 + \bar{\xi}_1^2)^3} \right] \frac{\partial G(\xi, \eta)}{\partial \bar{\xi}_1} d\bar{\xi}_1. \end{aligned}$$

It is clear that the first term on the right hand side is bounded since r_1 is fixed. Using Lemma 7.1 again, we have

$$\frac{\partial G(\xi, \eta)}{\partial \bar{\xi}_1} = -\frac{\bar{\xi}_1}{\pi(\bar{\xi}_1^2 + \eta_2^2)} + O(\ln(\bar{\xi}_1^2 + \eta_2^2)) + \frac{O(\eta_1)}{(\bar{\xi}_1^2 + \eta_2^2)^{1/2}}, \quad \xi \in S.$$

Replacing this equality into the second integral, we obtain

$$\begin{aligned} & \int_{-r_1}^{r_1} \frac{\bar{\xi}_1^2 [9\eta_2^4 - 14\eta_2^2 \bar{\xi}_1^2 + \bar{\xi}_1^4]}{(\bar{\xi}_1^2 + \eta_2^2)^4} G(\xi, \eta) d\bar{\xi}_1 \\ &= O(1) + \int_{-r_1}^{r_1} \left[\frac{5\eta_2^2 \bar{\xi}_1}{(\eta_2^2 + \bar{\xi}_1^2)^2} - \frac{\bar{\xi}_1}{\eta_2^2 + \bar{\xi}_1^2} - \frac{4\eta_2^4 \bar{\xi}_1}{(\eta_2^2 + \bar{\xi}_1^2)^3} \right] \frac{\bar{\xi}_1}{\pi(\bar{\xi}_1^2 + \eta_2^2)} d\bar{\xi}_1 \\ & - \int_{-r_1}^{r_1} \left[\frac{5\eta_2^2 \bar{\xi}_1}{(\eta_2^2 + \bar{\xi}_1^2)^2} - \frac{\bar{\xi}_1}{\eta_2^2 + \bar{\xi}_1^2} - \frac{4\eta_2^4 \bar{\xi}_1}{(\eta_2^2 + \bar{\xi}_1^2)^3} \right] \left[O(\ln(\bar{\xi}_1^2 + \eta_2^2)) + \frac{O(\eta_1)}{(\bar{\xi}_1^2 + \eta_2^2)^{1/2}} \right] d\bar{\xi}_1. \end{aligned}$$

The last integral can be estimated to be of the order $O((\ln \eta_2)^2)$. The first integral can be directly calculated which results in

$$\int_{-r_1}^{r_1} \frac{\bar{\xi}_1^2 [9\eta_2^4 - 14\eta_2^2 \bar{\xi}_1^2 + \bar{\xi}_1^4]}{(\bar{\xi}_1^2 + \eta_2^2)^4} G(\xi, \eta) d\bar{\xi}_1 = -\frac{1}{8\eta_2} + O((\ln \eta_2)^2).$$

Finally, we note that $f_a''(\eta_1) = f_a''(0) + O(\eta_1)$. Replacing this and the above equality into (73), we have

$$I_2 = \frac{f_a''(\eta_1)}{16\pi\eta_2} + O((\ln \eta_2)^2) = \frac{f_a''(0)}{16\pi\eta_2} + O((\ln \eta_2)^2).$$

References

- [1] T. Arens. Why linear sampling works. *Inverse Problems*, 20(1):163–173, 2004.
- [2] T. Arens and A. Lechleiter. The linear sampling method revisited. *Integral Equations and Applications*, 21(2):179–202, 2009.
- [3] M. Brignone, G. Bozza, R. Aramini, M. Pastorino, and M. Piana. A fully no-sampling formulation of the linear sampling method for three-dimensional inverse electromagnetic scattering problems. *Inverse Problems*, 25(1):015014, 20pp, 2009.
- [4] F. Cakoni and D. Colton. *Qualitative Methods in Inverse Scattering Theory*. Springer, 2006.
- [5] D. Colton and A. Kirsch. A simple method for solving inverse scattering problems in the resonance region. *Inverse Problems*, 12(4):383–393, 1996.
- [6] D. Colton and R. Kress. *Inverse acoustic and electromagnetic scattering theory*, volume 93 of *Applied Mathematical Sciences*. Springer-Verlag, Berlin, second edition, 1998.
- [7] G. Dassios and K. S. Karadima. Time harmonic acoustic scattering in anisotropic media. *Math. Methods Appl. Sci.*, 28(12):1383–1401, 2005.
- [8] M. Hanke. Why linear sampling really seems to work. *Inverse Probl. Imaging*, 2(3):373–395, 2008.
- [9] A. Kirsch and N. Grinberg. *The factorization method for inverse problems*, volume 36 of *Oxford Lecture Series in Mathematics and its Applications*. Oxford University Press, Oxford, 2008.
- [10] R. Kress. On the numerical solution of a hypersingular integral equation in scattering theory. *J. Comput. Appl. Math.*, 63(3):345–360, 1995.

- [11] J.-L. Lions and E. Magenes. *Non-homogeneous boundary value problems and applications. Vol. I.* Springer-Verlag, New York, 1972. Translated from the French by P. Kenneth, Die Grundlehren der mathematischen Wissenschaften, Band 181.
- [12] J. Liu and M. Sini. On the accuracy of the numerical detection of complex obstacles from far field data using the probe method. *SIAM J. Sci. Comput.*, 31(4):2665–2687, 2009.
- [13] J. J. Liu, G. Nakamura, and M. Sini. Reconstruction of the shape and surface impedance from acoustic scattering data for an arbitrary cylinder. *SIAM J. Appl. Math.*, 67(4):1124–1146 (electronic), 2007.
- [14] G. Nakamura and M. Sini. Obstacle and boundary determination from scattering data. *SIAM J. Math. Anal.*, 39(3):819–837, 2007.
- [15] N. T. Thành and M. Sini. An analysis of the accuracy of the linear sampling method for an acoustic inverse obstacle scattering problem. *Inverse Problems*, 26(1):015010 (29pp), 2010.
- [16] N. Valdivia. Uniqueness in inverse obstacle scattering with conductive boundary conditions. *Appl. Anal.*, 83(8):825–851, 2004.